nature ecology & evolution

Article

https://doi.org/10.1038/s41559-022-01921-w

Decoupling the skull and skeleton in a Cretaceous bird with unique appendicular morphologies

Received: 1 July 2022

Accepted: 3 October 2022

Published online: 2 January 2023

Check for updates

Zhiheng Li[1,2,4], Min Wang[1,2,4] ✉, Thomas A. Stidham[1,2,3] & Zhonghe Zhou[1,2]

The Cretaceous is a critical time interval that encompasses explosive diversifications of terrestrial vertebrates, particularly the period when the earliest-branching birds, after divergence from their theropod ancestors, evolved the characteristic avian Bauplan that led eventually to their global radiation. This early phylogenetic diversity is overwhelmed by the Ornithothoraces, consisting of the Enantiornithes and Ornithuromorpha, whose members evolved key derived features of crown birds. This disparity consequently circumscribes a large morphological gap between these derived clades and the oldest bird *Archaeopteryx*. The non-ornithothoracine pygostylians, with an intermediate phylogenetic position, are key to deciphering those evolutionary transformations, but progress in their study has been hampered by the limited diversity of known fossils. Here we report an Early Cetaceous non-ornithothoracine pygostylian, *Cratonavis zhui* gen. et sp. nov., that exhibits a unique combination of a non-avialan dinosaurian akinetic skull with an avialan post-cranial skeleton, revealing the key role of evolutionary mosaicism in early bird diversification. The unusually elongated scapular and metatarsal one preserved in *Cratonavis* highlights a breadth of skeletal plasticity, stemming from their distinct developmental modules and selection for possibly raptorial behaviour. Mapped changes in these two elements across theropod phylogeny demonstrate clade-specific evolutionary lability.

The assembly of the volant bird body plan from the ancestral dinosaurian condition is an enduring theme of interdisciplinary investigation in evolutionary biology, encompassing some of the most dramatic transformations morphologically, functionally and ecologically[1–4]. The ongoing discovery of early-branching avialans and their closest theropod relatives have advanced, but also have complicated our understanding of this evolutionary transition, because of the modular and heterogeneous assembly of typical derived avialan features documented by an imperfect fossil record along the line to birds[2,5,6]. In this Article, we describe a new early-diverging non-ornithothoracine pygostylian, *Cratonavis zhui* gen. et sp. nov., based on a complete skeleton from the Early Cretaceous Jehol Biota in China. This specimen preserves the plesiomorphic diapsid temporal configuration and non-avialan dinosaurian palatal complex. The primitive cranial morphologies stand in stark contrast with its derived set of post-cranial morphologies, reflecting the influence of mosaic evolution and biological experimentation deep within avialan phylogeny. The autapomorphic features preserved in this extinct species include a greatly lengthened scapula and hallux

[1]Key Laboratory of Vertebrate Evolution and Human Origins, Institute of Vertebrate Paleontology and Paleoanthropology, Chinese Academy of Sciences, Beijing, China. [2]Center for Excellence in Life and Paleoenvironment, Chinese Academy of Sciences, Beijing, China. [3]University of Chinese Academy of Sciences, Beijing, China. [4]These authors contributed equally: Zhiheng Li, Min Wang. ✉e-mail: wangmin@ivpp.ac.cn

coupled with a highly elongate first metatarsal, which are rarely seen in non-avialan paravians. Their evolutionary changes across the dinosaur–bird transition demonstrate how deeply conserved skeletal elements re-acquired evolutionary versatility.

Results

Systematic palaeontology

Avialae (Gauthier 1986; ref. [7])
Pygostylia (Chiappe 2002; ref. [8])
Jinguofortisidae (Wang et al. 2018; ref. [9])
Cratonavis zhui gen. et sp. nov.

Etymology

The generic name is derived from craton (referring to the destruction of North China Craton during the Early Cretaceous, an event that underpins the evolutionary setting of the Jehol Biota[10]) and Latin '*avis*' (bird). The specific name is in honour of Dr Rixiang Zhu for his pioneering work of the destruction of North China Craton.

Holotype

IVPP V31106 (housed at the Institute of Vertebrate Paleontology and Paleoanthropology, Chinese Academy of Science), a complete articulated skeleton with associated feathers (Fig. 1 and Supplementary Table 1).

Locality and horizon

Xiaotaizi Village, Lamadong Town, Jianchang Country, Liaoning Province, northeastern China; Early Cretaceous, Jiufotang Formation (~120 Ma (ref. [10])).

Diagnosis

A jinguofortisid that preserves the following synapomorphies of the Jinguofortisidae: fused scapulocoracoid; boomeranged-shaped furcula without a hypocleidium; proximal margin of the humerus centrally concave; and minor metacarpal bowed caudally. *Cratonavis* is distinguishable from other jinguofortisids on the basis of the following features (*asterisk denotes autapomorphy): ascending process of the maxilla perforated only by a maxillary fenestra; maxillary fenestra longer rostrocaudally than dorsoventrally; descending ramus of the lacrimal exhibiting a lateral flange*; squamosal process of the quadratojugal substantially longer (3×) than the jugal process; pterygoid with a caudodorsally directed quadrate ramus; prominent retroarticular process on the jaw; thoracic vertebral centra laterally excavated by broad fossae; scapula longer than the humerus; caudal end of the postacetabular process of the ilium dorsally deflected*; metatarsal I approximately 60% of the length of the tarsometatarsus*; and hallux bearing the longest non-ungual and ungual pedal phalanges*.

Description

IVPP V31106 is interpreted as an adult individual on the basis of complete fusion of all compound elements (synsacrum, pygostyle, tibiotarsus and tarsometatarsus), partially fused frontals and the absence of surface striations or pits that would indicate incomplete periosteal ossification[9,11,12]. The specimen is estimated to have a body mass of 666.16 g using an empirical equation based on the femoral circumferences (Methods)[13].

The premaxillae are fused rostrally, but their frontal processes are separated as in other early-diverging avialans (Fig. 2a,b and Extended Data Fig. 1). There are four premaxillary teeth on each side, and the rostral two are larger. As in *Archaeopteryx* and most non-avialan theropods[14,15], the broad ascending process of the maxilla is largely occupied by a triangular antorbital fossa (Fig. 2c), which is sharply rimmed ventrally as in the dromaeosaurid *Linheraptor*[16]. By contrast, that process is rostrocaudally restricted in other early avialans[17–20]. Like some troodontids (for example, *Saurornithoides* and *Zanabazar*)[21], the ascending process is perforated only by the maxillary fenestra as in enantiornithine *Zhouornis* (proportionately smaller in the latter)[22], and lacks the more rostrally positioned promaxillary fenestra present in *Archaeopteryx* and many non-avialan theropods[14–16,23,24]. The maxillary fenestra, separated from the antorbital fenestra by a stout interfenestral pila[24], is considerably longer rostrocaudally than dorsoventrally, opposite of the condition present in many maniraptorans, including *Archaeopteryx*[25,26]. The T-shaped lacrimal has short rostral and caudal rami that are otherwise prominent in most other theropods, including early-branching avialans (Extended Data Fig. 1)[16,18,27,28]. The descending process bears a lateral flange that is absent among other early avialans, but present in troodontids and dromaeosaurids[16,18,27,28]. A deep furrow runs along the caudodorsal corner of the lacrimal, probably demarcating the rostral edge of the orbit as some non-avialan theropods but absent in early-branching avialans[16,18,27,28]. As in some non-avialans theropods (for example, *Sinovenator* and *Dilong*)[29] and some early avialans (for example, *Archaeopteryx*[15] and *Falcatakely*[30]), the jugal has a caudodorsally oriented postorbital process that is longer than the quadratojugal process (Fig. 2 and Extended Data Fig. 1). Like *Falcatakely* and non-avialan theropods[16,31], but unlike *Archaeopteryx* and the juvenile enantiornithine IVPP V12707 (ref. [15,18]), a corneal process is absent from the caudal margin of the postorbital process. The L-shaped quadratojugal has an elongate squamosal process that is three times as long as the jugal process, and contrasts with the subtle difference among other early avialans, including *Archaeopteryx*, confuciusornithids and enantiornithines[15,18]. The triradiate postorbital is morphologically more similar to that of non-avialan theropods (for example, *Linheraptor*)[16,31] than that of *Archaeopteryx*[15] and more crownward taxa[18] in having stout frontal, squamosal and jugal processes (Fig. 2d). The squamosal appears to be rectangular, but details of its morphology are obscured by preservation (Fig. 2a). The quadrate has a bicondylar mandibular process as in other early avialans[18,20]. The preserved post-orbital elements show that *Cratonavis* retains the ancestral diapsid temporal configuration, with the orbit, and supratemporal and infratemporal fenestrae separated from one another as in non-ornithothoracine dinosaurs, and some enantiornithines (Fig. 2e)[18,23,31]. The frontals are partially fused with each other but are separated from the parietals. Fusion degree of the parietals cannot be ascertained.

The blade-like vomer has a dorsoventrally compressed and mediolaterally expanded premaxillary ramus, followed by a splint-like pterygoid ramus (Fig. 2f), and the bone is drastically different from that of *Archaeopteryx*[32], *Sapeornis*[17] and *Gobipteryx*[33]. The palatines, despite being incomplete, are notably large given the size of the skull. The two heavy palatines contact medially throughout their preserved lengths (Fig. 2b and Extended Data Fig. 1). In a manner like that found in non-avialan theropods and some enantiornithines[18,28,34,35], the pterygoid bears a large caudodorsally projecting quadrate ramus (Fig. 2g). A potential vestigial homologue of this structure is present in *Hesperornis*[36] and palaeognaths[37], and is completely absent in neognaths[38]. Given its preservation, it is unclear whether the quadrate ramus is forked caudally as in IVPP V12707 and non-avialan maniraptorans[18,34,35]. The palatine ramus of the pterygoid is dorsoventrally compressed and rapidly narrows rostrally. The basisphenoid–parasphenoid has an elongate, rostrally tapering parasphenoid rostrum (Supplementary Fig. 1). As in crown birds[37,38], but unlike IVPP V12707 and some non-avialan theropods[18,35], the ventral surface of the parasphenoid rostrum is convex. A distinct subsellar recess is present at the base of the parasphenoid rostrum as in IVPP V12707 and some non-avialan theropods (for example, *Velociraptor*)[18,24,25], but it is absent in crown birds[38] and some dromaeosaurids such as *Linheraptor*[16]. The basipterygoid processes are prominent and project ventrolaterally beyond the ventral level of the basisphenoid as in *Zhouornis*[22] and non-avialan theropods[18,23,37]. The right ectopterygoid preserves only its hook-shaped jugal process.

Similar to *Jeholornis* and *Sapeornis*[17,39], the dentary exhibits a reduced dentition in having three teeth restricted to the rostral region.

https://doi.org/10.1038/s41559-022-01921-w

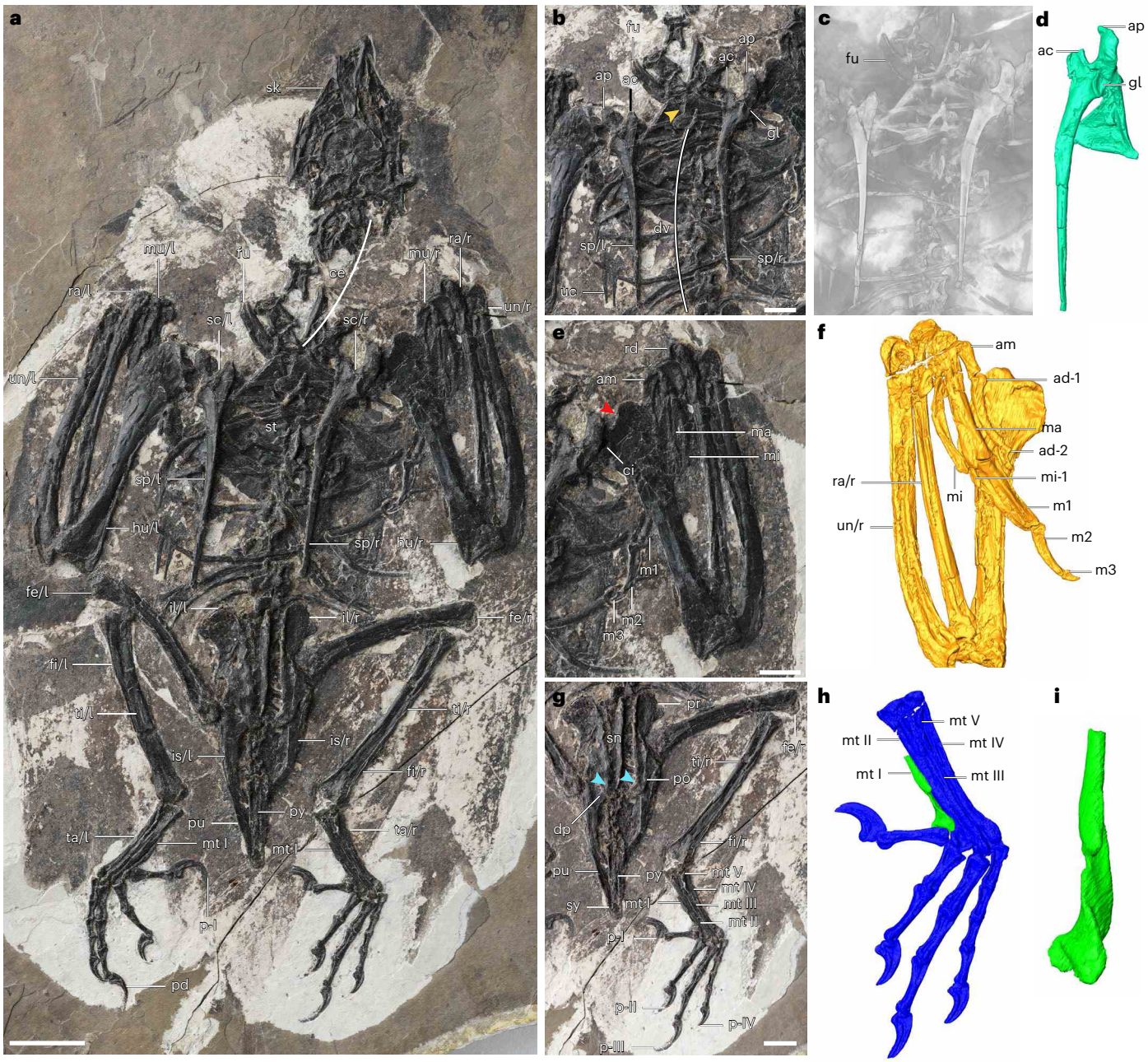

Fig. 1 | Holotype of *Cratonavis zhui*, IVPP V31106. a, Whole skeleton. **b**,**c**, Photograph (**b**) and CT (**c**) scan of the pectoral girdle. **d**, Digital reconstruction of the right scapulocoracoid. **e**,**f**, Photograph (**e**) and digital reconstruction (**f**) of the right forelimb. **g**, Pelvis and right hindlimb. **h**,**i**, Digital reconstruction of the right foot in plantar view (**h**), and metatarsal I in medioplantar view (**i**). ac, acromion process; ad-1, alular digit phalanx-1; ad-2, alular digit phalanx-2; am, alular metacarpal; ap, acoracoid process; ce, cervical vertebra; ci, capital incision; dp, dorsal process of ischium; dv, dorsal vertebra; fe, femur; fi, fibula; fu, furcula; gl, glenoid; hu, humerus; il, ilium; is, ischium; m1 to m3, major digit phalanx-1 to 3; ma, major metacarpal; mi, minor metacarpal; mi-1, minor digit phalanx-1; mt I–V, metatarsals I to V; mu, manus; ra, radius; sc, scapulocoracoid; sp, scapula; ta, tarsometatarsus; ti, tibiotarsus; un, ulna; p-I to p-IV, pedal digits I to IV; po, postacetabular process; pr, pre-acetabular process; pu, pubis; py, pygostyle; sk, skull; sn, synsacrum; st, sternum; sy, symphysis of pubes; uc, uncinate process; l/r, left/right side. Yellow arrowhead in **b** denotes the cranial cleft of the sternum, red arrowhead in **e** indicates the concave proximal margin of humerus and blue arrowheads in **g** denote the dorsal deflection of the distal ilium. Scale bars, 10 mm (**a**, **b**, **e** and **g**).

However, the tooth row extends to the rostrocaudal midpoint in other toothed avialans, including *Jinguofortis*[9,20,31]. The dentary is biforked caudally, with a ventral ramus longer than the dorsal one as in confuciusornithids[19]. The angular, surangular and articular are loosely fused to one another. As in some crown birds such as galloanserines[38], a large retroarticular process projects caudodorsally well beyond the caudal margin of the articular region (Fig. 2a,b), and it is considerably longer than the condition in other early-branching avialans[9,17,19,20].

The robust and boomeranged-shaped furcula is nearly identical to that of other jinguofortisids[9]. The scapula and coracoid are fused into a single scapulocoracoid element (Fig. 1b–d and Extended Data Fig. 2), a plesiomorphic or probably homoplastic condition that is widely distributed in non-avialan dinosaurs and pterosaurs but hitherto has been reported only in the early-diverging pygostylian jinguofortisids and confuciusornithids among Mesozoic avialans[9,23,40]. The scapula is longer than the humerus, but the latter is much longer in

https://doi.org/10.1038/s41559-022-01921-w

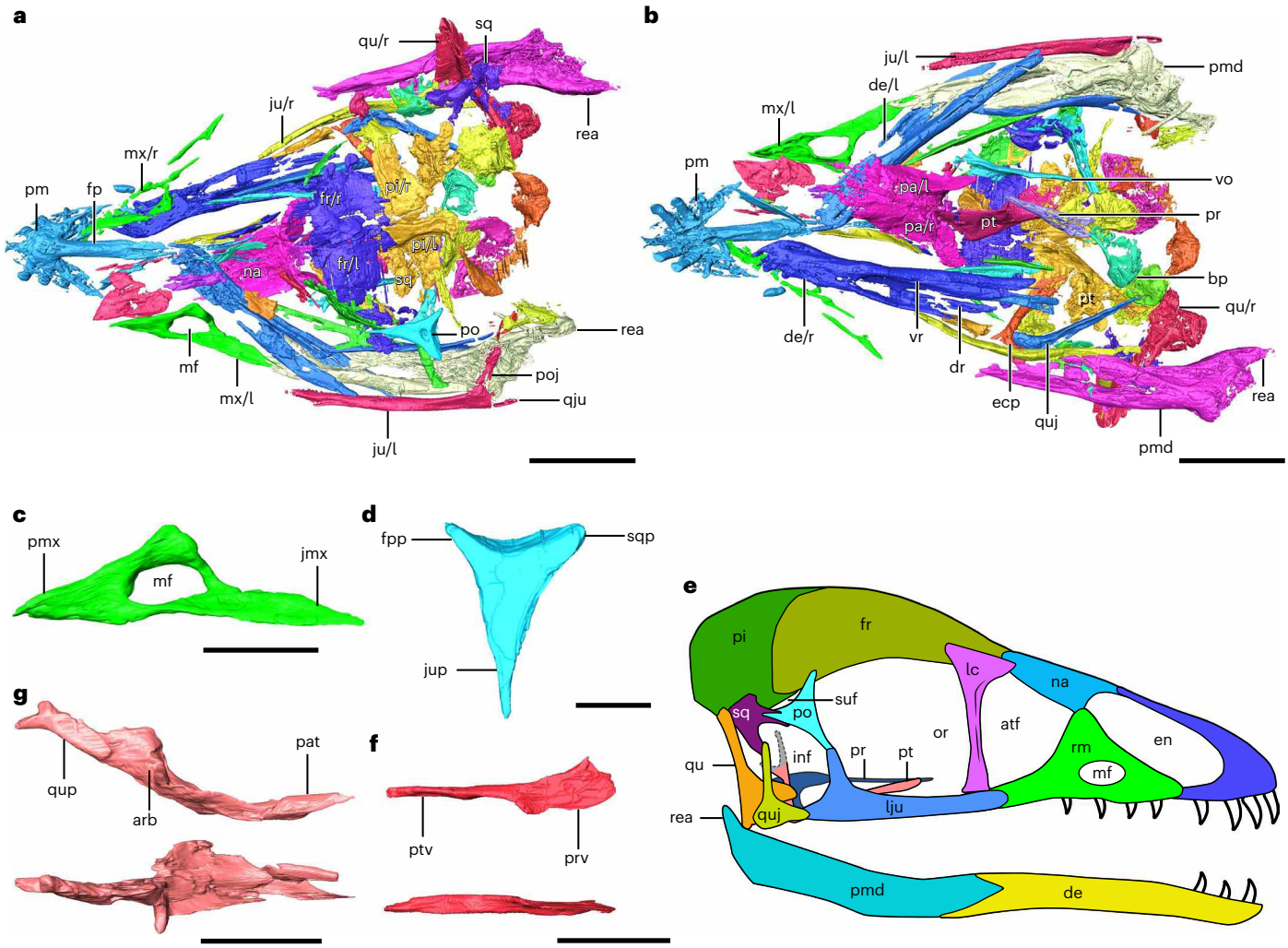

Fig. 2 | Cranial anatomy of *Cratonavis*. **a**–**d**,**g**,**f**, Digital reconstruction of the entire skull in dorsal (**a**) and ventral (**b**) view, the left maxilla (**c**, lateral view), left postorbital (**d**, lateral view), right vomer (**f**: upper, dorsal view; lower, lateral view) and right pterygoid (**g**: upper, lateral view; lower, dorsal view). **e**, Interpretative skull reconstruction. arb, articular facet for basipterygoid process; atf, antorbital fenestra; bp, basipterygoid process; de, dentary; dr, dorsal ramus of dentary; ecp, ectopterygoid; en, external naris; fp, frontal process of premaxilla; fpp, frontal process of postorbital; fr, frontal; inf, infratemporal fenestra; jmx, jugal process of maxilla; ju, jugal; jup, jugal process of postorbital; mf, maxillary fenestra; mx, maxilla; na, nasal; or, orbit; pa, palatine; pat, palatine ramus; pi, parietal; pm, premaxilla; pmd, post-dentary mandible; pmx, premaxillary process of maxilla; po, postorbital; poj, postorbital process of jugal; pr, parasphenoid rostrum; prv, premaxillary ramus of vomer; pt, pterygoid; ptv, pterygoid ramus of vomer; qju, quadratojugal process of jugal; qu, quadrate; quj, quadratojugal; qup, quadrate ramus of pterygoid; rea, retroarticular process; sqq, squamosal process of quadratojugal; sq, squamosal; sqp, squamosal process of postorbital; suf, supratemporal fenestra; vo, vomer; vr, ventral ramus of dentary; l/r, left/right side. Scale bars, 10 mm (**a** and **b**), 5 mm (**c**, **f** and **g**) and 2.5 mm (**d**).

most maniraptorans including early avialans (Supplementary Table 2). The large acromion process is rectangular in outline and is dorsoventrally as wide as the midshaft of the scapular blade. In contrast, the acromion is small and tapers cranially in *Archaeopteryx*, *Jeholornis* and confuciusornithids[14,41,42]. The scapular blade gently tapers distally, and lacks the caudal expansion present in confuciusornithids[43]. The glenoid fossa across the scapulocoracoid faces laterodorsally (Fig. 1d), indicating that the forelimb could be elevated above the dorsum. As in *Chongmingia* and ornithothoracines, the coracoid is strut-like and expands mediolaterally along its sternal half. The acrocoracoid process curves medially, and together with the acromion process of the scapula may have helped to form a structure that is functionally analogous to the triosseal canal in crown birds, serving as a passage for the tendon of the musculus supracoracoideus to elevate the wing during the flight upstroke[38]. Like *Jinguofortis* and confuciusornithids[9,44], the sternum is formed by two bilaterally fused plates with a cranial cleft, and the bone is mediolaterally wider than craniocaudally long (Fig. 1a). The caudal margin of the sternum is rounded as in *Jeholornis*, and it contrasts with the V-shaped form present in confuciusornithids[42,44].

The proximal end of the humerus is strongly deflected ventrally with the ventral tubercle ventral to the humeral shaft, exceeding the degree of displacement observed in other early avialans[15,39,43]. The proximal margin is highly concave centrally and convex caudally (Fig. 1e,f), an unusual feature shared with other jinguofortisids and independently developed in enantiornithines among stemward avialans[9,45,46]. A bulbous humeral head is evolutionarily missing, and the proximal articular surface is roughly C-shaped with an elongate ridge marking its caudal margin raised distinctly above the caudal surface of the proximal humerus. The proximal radius preserves a bicipital tubercle (Extended Data Fig. 2), as in *Confuciusornis* and some non-avialan theropods[47]. As in *Jinguofortis*[9], but unlike other stem avialans[14,45], the capital incisure is distinctly deep and wide. Like most volant avialans[6], the ulna is longer than the humerus. The semilunate carpal is fused

with the proximal ends of the major and minor metacarpals, forming a carpometacarpus. The alular metacarpal is fused only proximally with the carpometacarpus. Like other jinguofortisids and *Jeholornis*[46], the minor metacarpal is strongly bowed caudally, defining a wide intermetacarpal space (Fig. 1f and Extended Data Fig. 2). In contrast, the minor metacarpal is straight in other early avialans[14,15,19,27,46]. The minor digit preserves only a single, wedge-shaped phalanx, suggesting that the manual phalangeal formula is probably 2–3–1.

Like confuciusornithids and some non-avialan theropods (for example, tyrannosaurids, ornithomimids, dromaeosaurids and oviraptorids)[48,49], the cranioventral end of the ilium protrudes ventrally almost level with the pubic peduncle, defining a deep concave ventral margin in lateral view. This ventral margin is nearly straight in other non-ornithothoracine avialans[9,41,50]. The postacetabular process terminates with a blunt distal end that curves dorsomedially (Fig. 1g and Extended Data Fig. 3). Given the same morphology preserved on both ilia, we suggest this dorsomedial deflection is genuine. No comparable condition has hitherto been found in other early avialans or non-avialan theropods[23,49].

The stout femur measures approximately 90% of the tibiotarsus in length. The fibula extends distally and almost contacts the lateral condyle, a plesiomorphic character retained in stemward avialans but rarely seen in more crownward taxa[15]. As in other stemward pygostylians[9,43], metatarsals II–IV are co-planar and fused proximally with the distal tarsals, but they remain separate along their distal lengths (Fig. 1h,i). The most striking feature of *Cratonavis* is the presence of a highly elongate metatarsal I, measuring approximately 56% the tarsometatarsus in length that is surpassed only by the dromaeosaurid *Balaur* (60%) among described theropods (Supplementary Table 2). Specifically, this ratio is well below the ratio of 30% found in most Mesozoic avialan and non-avialan theropods, but it is slightly larger in the Pengornithidae (32–39%). As in most non-avialan theropods[23,51], metatarsal I articulates with the medial surface of metatarsal II at its mid-length, rather than being distally positioned as in other maniraptorans, including avialans[27,43,52,53]. The distal third of metatarsal I is deflected plantarly to form a ball-like articular surface (Fig. 1i). As in other stemward avialans[15,46,52], metatarsal V is vestigial and unfused with other metatarsals. The ungual phalanges are strongly recurved and have well-developed flexor processes that are most prominent in digits I and II. The proximal and ungual phalanges of the hallux are longer than those of other digits (Fig. 1h), a unique feature unknown in maniraptorans, including stemward avialans[15,41,43] (for additional description including the vertebral column, see Supplementary Note 1).

Phylogenetic position of *Cratonavis*

The phylognetic analysis recovered 4,352 most parsimonious trees with a length of 1,422 steps (consistency index 0.273, retention index 0.663). *Cratonavis* is resolved as the sister taxon to *Chongmingia*, which is united with *Jinguofortis* to form the monophyletic clade Jinguofortisidae in the strict consensus tree (Fig. 3). Jinguofortisidae is supported by nine synapomorphies: thoracic vertebrae less than 11 (character 56:2); proximal haemal arches absent (character 74:2); proximal margin of the humerus concave centrally (character 123:1); intermetacarpal space twice as wide as the width of the minor metacarpal (character 164:1); manus and humerus subequal in length (character 176:1); postacetabular process more than half the depth of the pre-acetabular process (character 186:0); hallux ungual larger than that of other pedal digits (character 243:2); fused scapulocoracoid (character 2,248:0); and proximal phalanx of alular digit shorter than or equivalent to the proximal phalanx of the major digit (character 250:1). The new topology is relatively well resolved, with the inter-relationships of major clades consistent with recent phylogenetic work[54–56]. Jinguofortisidae, Confuciusornithidae and *Sapeornis* form a polytomy as the closest outgroup to the Ornithothoraces, which consists of the Enantiornithes and Ornithuromorpha (Ornithuromorpha refers to the first ancestor of Neornithes that is not also an ancestor of the Enantiornithes, and all of its descendants[57]).

Evolutionary changes of scapula and metatarsals in Theropod

The most notable feature of *Cratonavis* is the presence of highly elongate scapula and first metatarsal. To quantify the changes of these two elements across theropod tree, we applied phylogenetic comparative analyses. The body size and phylogenetically corrected scapula length is more variable in non-avialan theropods, and within avialans scapula elongation took place independently in jinguofortisids and some ornithuromorphs (Fig. 4a and Extended Data Figs. 4 and 5). Scapula length shows a weak but significantly positive allometric relationship to the lengths of the humerus (slope: 1.19; $P < 0.01$) and femur (slope: 0.86; $P < 0.01$) with phylogenetic dependence corrected or not (Fig. 4 and Extended Data Fig. 6). *Cratonavis* emerges as a distinctive outlier, falling well above the 95% confidence interval of the regression line, and thus represents the taxon with the longest scapula given the same humerus/femur length among theropods analysed here.

There is a general trend in the reduction of metatarsal I along the phylogenetic lines towards avialans, but therizinosaurids and derived dromaeosaurids exhibit a reversal (Fig. 5a and Extended Data Fig. 7). Among stemward avialans, a re-elongation of metatarsal I convergently occurs in jinguofortisids and the enantiornithine clade Pengornithidae. Enantiornithines overall have a longer metatarsal I than that of early ornithuromorphs, and this difference reflects ecological divergence between these two clades (largely arboreal versus largely terrestrial or aquatic)[55]. We further trace the length ratio of metatarsals I and III across theropod phylogeny (Extended Data Figs. 8 and 9). The results indicate that the length ratio present in stemward avialans was established deep in early coelurosaur evolution, and then it remained relatively stable along the line to avialans with a few exceptions (for example, therizinosaurids and derived dromaeosaurids). This result is corroborated by a significantly high phylogenetic signal exhibited by metatarsal I (both length and ratio) quantified by Blomberg's K and Pagel's λ (refs. [58,59]) in all theropods, but the phylogenetic signal is diminished along the line to paravians (Fig. 5, Extended Data Figs. 8 and 9, and Supplementary Table 3).

Discussion

As one of the earliest-branching pygostylians, jinguofortisids (~8 million years of duration for the known members) preserve a suite of unique morphologies that is further complicated by *Cratonavis*. *Cratonavis* has a heavily built skull that is morphologically more like that of non-avialan theropods than most contemporaneous avialans, attesting to the presence of the plesiomorphic diapsid temporal configuration (temporal and postorbital bars completely separating the orbit, and supratemporal and infratemporal fenestrae; Fig. 2e). These elements are functionally vital to modern avian cranial kinesis that enables the upper jaw to be moved independently of the braincase and lower jaw[60,61], and it is an evolutionary novelty underpinning the much of the enormous ecological success of crown birds[6]. However, all of these bones retain the typical non-avialan dinosaurian morphologies with little modifications, demonstrating that the skull of *Cratonavis* was akinetic as in some other early-diverging avialans. Our study reinforces the latest hypothesis that a true kinetic cranium is absent over a large part of Cretaceous avialan history[5,17,18,62], and during that period the skull was evolutionarily and functionally conservative.

Cratonavis also shares other particular cranial features with non-avialan theropods, including the ascending process of the maxilla only perforated by the maxillary but not promaxillary fenestra as in some troodontids[21], lacrimal bearing a lateral flange as in dromaeosaurids and troodontids[16,28], and the large squamosal and vomer[20,25]. In contrast, the post-cranial skeleton of *Cratonavis* displays derived avialan features, including a fused pygostyle, an ossified sternum, an elongate forelimb, reduced manual phalanges and a reversed hallux.

https://doi.org/10.1038/s41559-022-01921-w

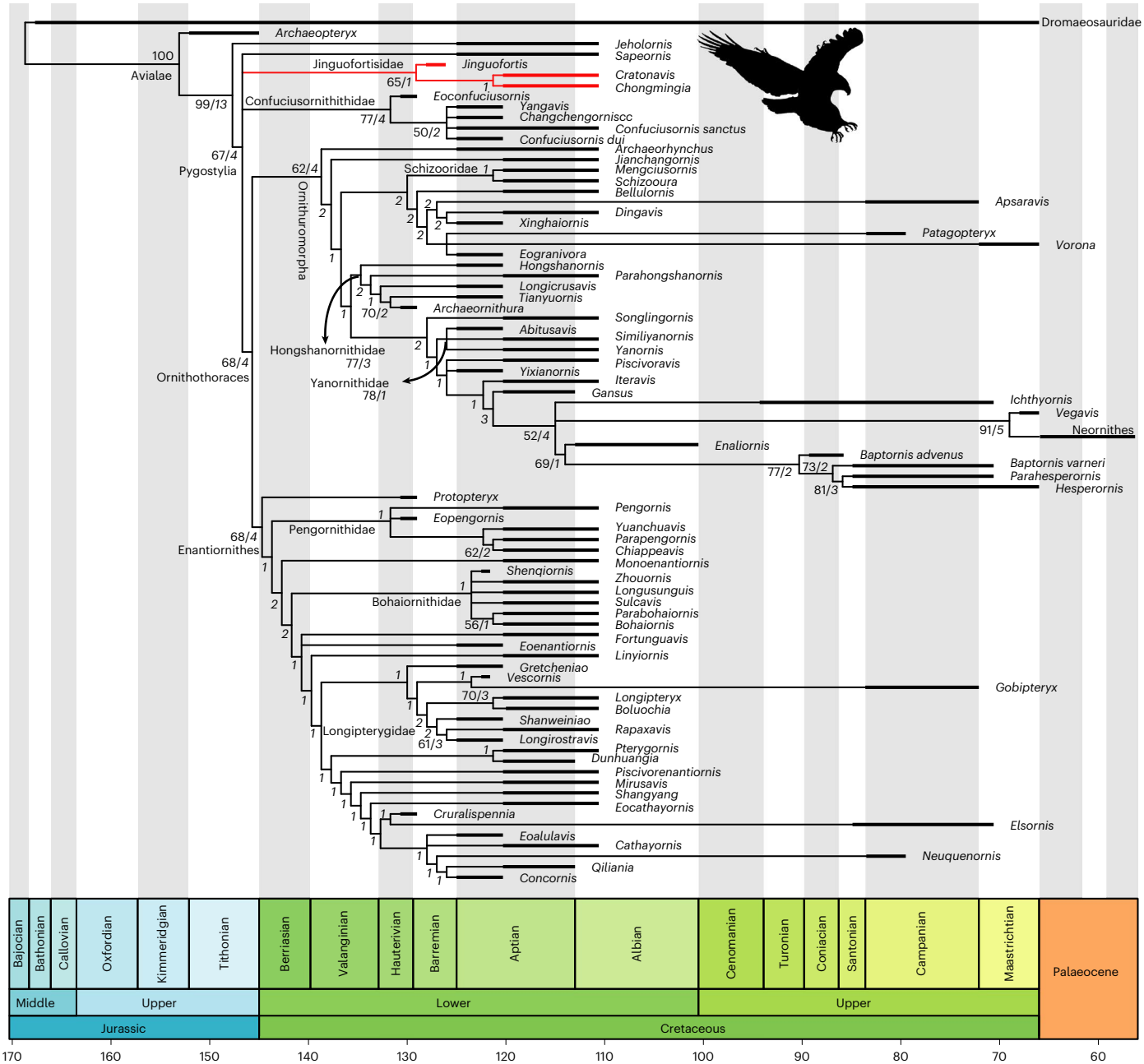

Fig. 3 | Time-calibrated Mesozoic avialan phylogeny showing the position of *Cratonavis*. The absolute frequency of bootstrap and Bremer support values are indicated in normal and bold italic formats near corresponding nodes, respectively.

The combination of a non-avialan dinosaurian skull and avialan post-cranial skeleton documented in *Cratonavis* adds to the tally of examples where avialan evolution has been shaped deeply by mosaicism[1,5,30], and this heterogeneity is notably conspicuous in differences between the cranial and post-cranial regions.

One of the unique features of *Cratonavis* is the presence of a highly elongate scapula that exceeds the humerus in length, a condition rarely seen in Mesozoic paravians except two stemward ornithuromorphs (*Yixianornis* and *Apsaravis*; Supplementary Table 2)[23,63]. The scapula is functionally integrated into avian flight system as a centre of muscle attachments that conveys stability and flexibility to the flight mechanism[64]. This bone underwent extensive evolutionary modifications (for example, position, shape and size) in the bird line when the primary locomotor strategies shifted from cursoriality to flight[65]. Despite its functional significance, only a few attempts have been made to explore its evolutionary pathway towards birds[66,67].

Our study shows that scapula length is more variable in non-avialan theropods, and within avialans scapula elongation took place independently in jinguofortisids and some ornithuromorphs (Fig. 4a and Extended Data Fig. 5). We explore possible explanations for the surprisingly elongate scapula present in *Cratonavis*. The costal surface of scapular blade serves as the attachment site for musculus scapulohumeralis caudalis (*shca*) that inserts on the proximocaudal side of humerus[68]. In many crown birds, *shca* is the third-largest flight muscle that retracts and adducts the wing, assisting the pectoralis muscle in completion of the whole cycle of the downstroke[6,68]. As such, the shape and length of the scapular blade vary greatly among taxa with different flight styles. For example, the blade in penguins and the great auk is

https://doi.org/10.1038/s41559-022-01921-w

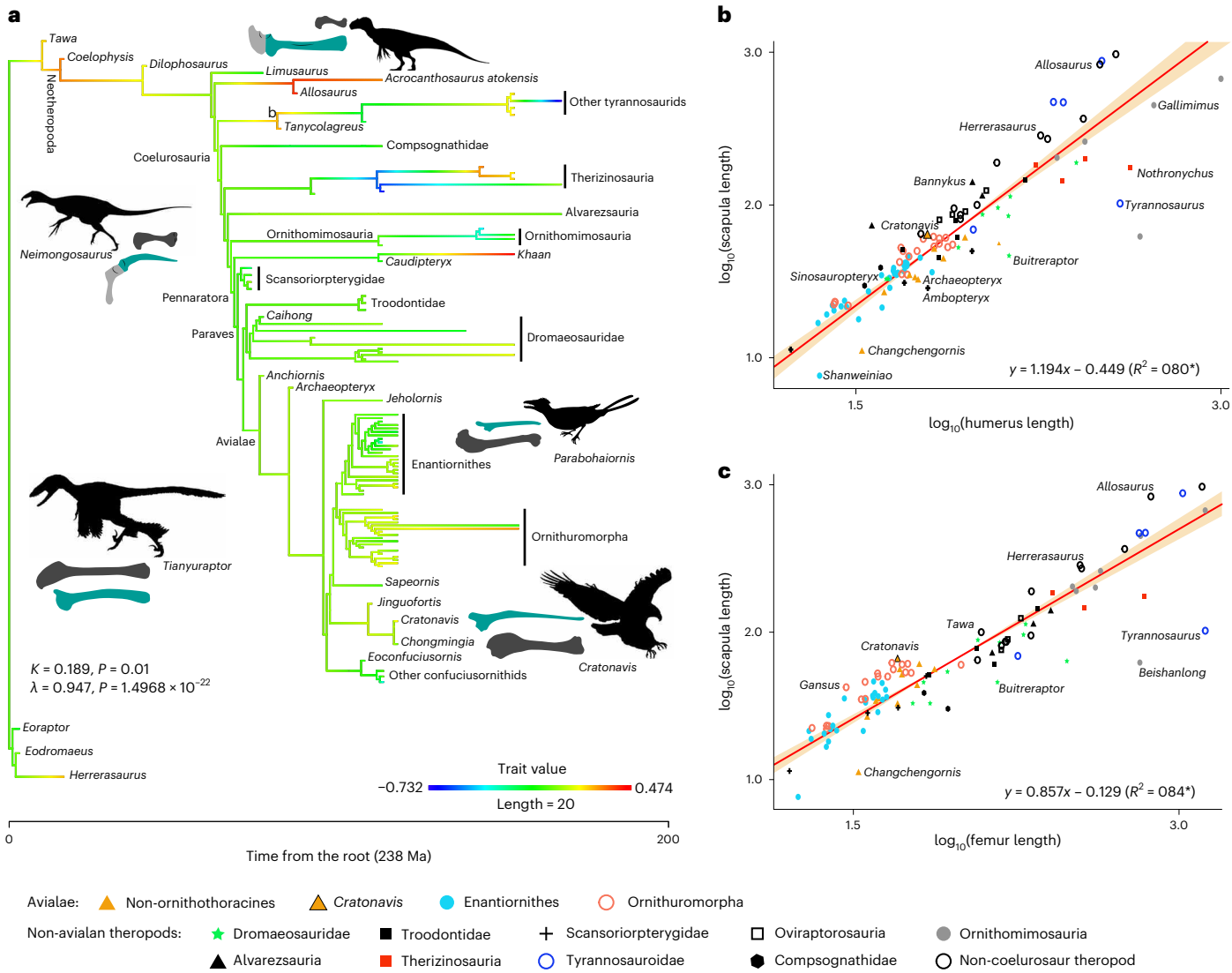

Fig. 4 | Evolution of scapula across theropod dinosaurs. a, Scapula length changes among major theropod groups (line drawing of scapulocoracoid/scapula scaled with humerus in selected taxa; for phylogenetic backbone, see Extended Data Fig. 4; for complete results, see Extended Data Fig. 5). **b**,**c**, Scaling relationships of scapula–humerus length (**b**), and scapula–femur length (the light surface denotes the 95% confidence interval) (**c**). Squared correlation coefficient (R^2) was statistically tested against zero (*indicates a two-sided *P*-value threshold <0.01).

expanded (increasing the area for *shca* attachment) to exert enough force to rotate the forelimb underwater[68,69]. The elongate scapula in *Cratonavis* may not only increase the attachment area but also increase the lever arm length, augmenting the mechanical advantage of *shca* for humerus retraction/rotation to produce forward thrust. Members of Galliformes may prove to be modern analogues because they also have a long scapula. They flap their wings rapidly to escape predators with near-vertical take-off from the ground surfaces[68]. The presence of a highly elongate scapula in *Cratonavis* probably compensated for the absence of an ossified sternal keel, which provides additional surface for the attachment of the pectoralis muscle, and this extinct species represents biological experimentation in volant behaviour. It is worth noting that stemward avialans exhibit numerous flight-related modifications to compensate for their underdeveloped flight apparatus, and some of these features are unknown among crown birds, such as the large deltopectoral crest with an elliptical fenestra[4,43].

The most remarkable and unique feature of *Cratonavis* is the enlarged and functional hallux that somehow resembles the condition observed in the enigmatic Late Cretaceous dromaeosaurid *Balaur*[70]. The hallux in *Cratonavis* and *Balaur* is enlarged via both the elongation of the metatarsal and phalanges, but the phalanges are enlarged to a greater degree in *Cratonavis*, resulting in the longest non-ungual and ungual phalanges in the foot, a condition unknown among other paravians. Morphometric analysis using ecological-related measurements shows that *Cratonavis* falls into the morphospace of modern arboreal birds and birds of prey (Fig. 5b and Extended Data Fig. 10). Thus, the autapomorphic pedal morphology in *Cratonavis* probably relates to its arboreal or possibly raptorial behaviour. The increasing lengths of the distal phalanges of pedal digit IV also point to a grasping or perching foot.

Pedal morphology is remarkable diverse and has been considered a textbook example of adaptive variation[71]. Previous studies have focused mainly on the middle three metatarsals across theropod evolution[72], leaving a large gap in our understanding of how the hallux has achieved its novel functional morphology in living birds that ranges across diverse functions such as perching, grasping and manipulating[73]. An unreduced metatarsal I is plesiomorphic for Saurischia, and it remains in contact with the ankle ancestrally[51,53]. Ceratosauria and

https://doi.org/10.1038/s41559-022-01921-w

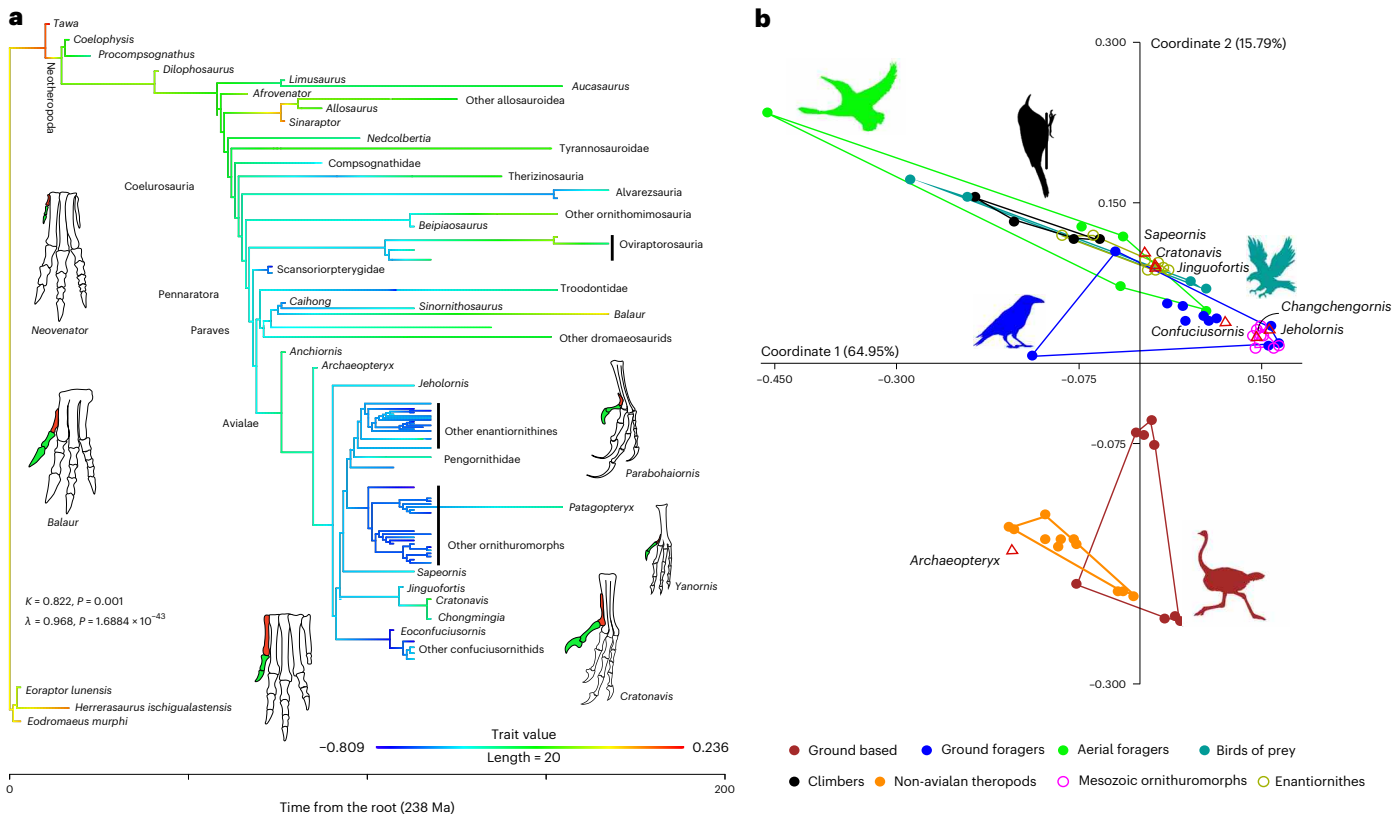

Fig. 5 | Evolution of metatarsals across theropod dinosaurs and ecological inference of *Cratonavis*. **a**, Changes of metatarsal I length along the line to early avialans (metatarsal I and hallux coloured in red and green, respectively; for complete results, see Extended Data Fig. 7). The phylogenetic signals were quantified using the Blomberg's *K* and Pagel's *λ* with *P* value of the likelihood radio test. **b**, Ecomorphospace based on the binary plot of the first two principal coordinate axes.

later-branching taxa show varying degrees of reduction in this element, ranging from losing contact with the ankle to becoming completely absent in some groups[23,51,53]. Our comparative analyses show that there is a general trend in the reduction of metatarsal I along avialan stem lineages, and the length ratio present in early avialans was established deep in early coelurosaur evolution. Therefore, we posit that metatarsal I had been subjected to selection favouring of a short form, and that the bone lost its evolutionary lability once an optimal size was reached. A reduced metatarsal I and hallux are not unusual among vertebrates with enhanced cursoriality, including non-avialan theropods such as ornithomimosaurs[72]. Interestingly, the phylogenetic signal of metatarsal I is diminished when only paravians are considered, and that difference suggests an increased evolutionary lability (Extended Data Fig. 8b and Supplementary Table 3)[74], which may have resulted from conflicting and dual demands associated with the direct employment of the hallux in locomotion and feeding (perching, climbing, grasping and so on) in early avialans and their closest paravian relatives[53,72,73]. The recovered evolutionary patterns of the scapula and metatarsals manifest how deeply conserved skeletal units break constraints given the dynamic interplay among developmental systems, natural selection and ecological/functional opportunity.

Methods

CT imaging

IVPP V31106 was scanned using the industrial computed tomography (CT) scanner Phoenix v-tome-x at the Institute of Vertebrate Paleontology and Paleoanthropology in Beijing. The skull was scanned with beam energy of 150 kV and a flux of 135 μA at a resolution of 16.682 μm. The post-cranial region was scanned with beam energy of 160 kV and a flux of 140 μA at a resolution of 39.983 μm. The resulting scanned images were imported into Avizo (v. 9.2.0) for digital segmentation, rendering and reconstruction.

Phylogenetic analysis

The systematic position of IVPP V31106 was investigated using a comprehensive data matrix targeting the phylogeny of Mesozoic avialans[55]. The data matrix consists of 280 morphological characters and 82 taxa, including nearly all well-recognized Mesozoic avialans ($n = 79$; Supplementary Information). The data matrix was analysed under equally weighted parsimony using the TNT software package (v.1.5) (ref. [75]). The New Technology search method with sectorial search, ratchet, tree drift and tree fusion was applied to search the most parsimonious tree, with the minimum-length tree found in ten replicates to recover as many tree islands as possible. The resulting most parsimonious trees were subjected to a second round of branch swapping using the traditional tree-bisection-reconnection algorithm to explore treespace more extensively. The absolute frequency of the bootstrap was calculated using 1,000 replicates using the same settings as the primary search, and the Bremer support values were calculated using the Bremer script embedded in TNT.

Appendicular element length dataset of theropods

To quantify the changes of the lengths of the scapula and metatarsal I across theropod phylogeny, particularly along the line to Mesozoic avialans, a dataset of the lengths of the scapula, metatarsal I, humerus, femur and metatarsal III from major groups of theropods was assembled from the literature and using first-hand measurements (Supplementary Table 2). The lengths of the latter three limb elements were

collected to investigate a potential allometric relationship across major theropod clades, and quantify the relative elongation/reduction of the scapula and metatarsal I. All included specimens were adults or subadults with reference to the original literature, and exhibit fusion of the compound bones and the well-ossified limb bone periosteal surfaces[9,11,12]. Given the uncertainty of scaling relationships of limb sizes, only specimens that preserve the complete length of the scapula–humerus–femur (for scapula analysis) and metatarsal I–metatarsal III–femur (for metatarsal analysis) were included. The length dataset contains 140 taxa, spanning nearly the whole spectrum of theropod diversity (including Mesozoic avialans). All of the length measurements were $\log_{10}$ transformed to normalize the distribution before downstream phylogenetic comparative analyses.

Body mass estimate

The body mass of *Cratonavis* holotype (IVPP V 31106) and other specimens included in the length dataset was estimated using the empirical scaling relationship of the circumference of the femur with body mass derived from living bipedal tetrapods[13]. For specimens that are preserved in two dimensions, the circumference was estimated using the equation derived from the diameter of the femoral shaft[76]. The body mass data were used in the following comparative analyses to account for size-dependent limb measurements.

Time-scaled phylogeny of theropods

A composite super tree of the taxa included in the length data was assembled as a backbone using the present phylogenetic result (for Avialae) combined with recent phylogenetic studies (for non-avialan theropods)[23,77–80]. To account for problematic taxa with competing phylogenetic placements in different hypotheses, and inter-relationships among derived members of some clades (for example, Allosauroidea and Compsognathidae), branches subtending to those taxa were collapsed as polytomies. The polytomies of the super tree were randomly resolved using the multi2di function of the R ape package (Extended Data Fig. 4)[81]. The completely resolved super tree was time scaled using tip dates bracketed by the first and last appearance datum of the geological stages or epochs in which each taxon were collected[82]. Zero-length branches were smoothed using the 'minimum branch length' embedded in the timePaleoPhy function in the R package paleotree[83], which sets a minimum branch length of one million years.

Comparative analyses of scapula length variation in theropods

We conducted phylogenetic comparative analyses to estimate changes in the scapula length across theropod phylogeny. To account for size dependence and non-independence in trait values between species due to shared history[84], we calculated residuals from a least-squares regression of the $\log_{10}$-transformed scapula length against $\log_{10}$-transformed body mass using the phyl.resid function in the R package phytools[85]. The size and phylogenetically corrected scapula length data were then projected on the time-scaled super tree to visualize the changes of scapula length among major theropod groups (Fig. 4a). The phylogenetic signal of scapula length was quantified by Blomberg's K and Pagel's λ (refs. [59,86]). The obtained K and λ were subjected into 1,000 randomizations test to compute a significance value (P). All of these steps were conducted using the phylosig function in the R package phytools[85].

To investigate the potential scaling relationship between the scapula and humerus, and between the scapula and femur, two independent regression analyses were performed. Given potential measurement errors in both variables (here scapula and humerus/femur), we used the standardized major axis (SMA) regression to investigate the scaling relationship between $\log_{10}$-transformed scapula and humerus lengths, and $\log_{10}$-transformed scapula and femur lengths, respectively (Fig. 4b,c). The strength of the correlation between the given variables was quantified by the coefficient of determination values (R^2) and statistical significance of those correlations from ordinary least-square regression. The obtained correlations were then tested to see if they were statistically significantly different from an isometry (slope = 1). The SMA and the statistical tests were conducted using the sma function in the smatr package[87] and the lmodel2 package[88]. Next, we tested if the recovered scaling relationships could be biased by phylogenetic non-independence (Extended Data Fig. 6). The log-transformed data were fed into a phylogenetic generalized least squares (pgls) using the nlme package[89].

Inference of ecological adaptation of *Cratonavis*

The exploration and reconstruction of ecology of extinct animals is notoriously challenging in palaeontology. It is common to make ecological inference on the basis of key ecomorphological features such as pedal morphology, or quantitative measurements such as limb proportions. Here we followed a previous study[90] using a suite of ecological indicative traits including quantitative measurements (for example, crural index: tibiotarsus/femur length for non-avialan theropods, and tarsometatarsus/tibiotarsus length for avialans; relative length of pedal phalanges of digit III) and descriptive parameters (for example, degree of hallux reversion and pedal claw curvature), to explore the palaeoecology of *Cratonavis* and other early avialans (Supplementary Table 4). These data were added into the original dataset[90], which includes modern birds that exhibit different ecological adaptations. A principal coordinate analysis was performed. The first two principal coordinate axes explained >80% of the variance, and were used to constructed an ecomorphospace (Supplementary Table 5). *Cratonavis* and *Jinguofortis* are spaced widely from *Archaeopteryx* and non-avialan theropods, and fall into the ecomorphospace of modern arboreal birds and birds of prey (Fig. 5b). We also conducted canonical variate analysis to infer the ecology of *Cratonavis* using the fda function in the R package mda[91]. The modern bird data were fed into canonical variate analysis as the training data to recover discriminable variables that can be used to classify these different ecological groups. Among the modern data, 87.5% could be correctly assigned to their original ecological groups (Extended Data Fig. 10). We then subjected *Cratonavis* into the resulting discriminant function, and *Cratonavis* was assigned to the 'arboreal' group, consistent with the principal coordinate result.

Comparative analyses of metatarsal I length variation in theropods

First, we calculated size and phylogenetically corrected $\log_{10}$-transformed metatarsal I lengths using the same procedure as in the scapula analysis outlined above. The length residues were mapped onto the time-scaled theropod phylogeny to illustrate how this element changes in length among major theropod lineages using the contMap function in the R package phytools[85]. Secondly, the length ratio of metatarsal I to III was mapped onto the time-scaled phylogeny after accounting for phylogenetic non-independence. These two mapping approaches could collectively demonstrate the tempo and patterns of metatarsal I length variations in 'absolute' and 'proportional' perspectives. All of these results clearly show that *Cratonavis* has the longest first metatarsal among equally sized theropods. Scaling relationship between metatarsals I and III length was analysed using the pgls regression method (Extended Data Fig. 9). The phylogenetic signals of both $\log_{10}$-transformed metatarsal I length and length ratio of metatarsal I to III were quantified using the Blomberg's K and Pagel's λ (refs. [59,86]), followed by a randomization test. K and λ were calculated for theropod as a whole and for the subgroups Coelurosauria, Maniraptoriformes, Pennaraptora and Paraves, respectively, to explore how the phylogenetic signal changes close to the origin of Avialae.

Reporting summary

Further information on research design is available in the Nature Research Reporting Summary linked to this article.

Data availability

The specimen (IVPP V31106) described in this study is archived and available on request from the Institute of Vertebrate Paleontology and Paleoanthropology (IVPP), Chinese Academy of Sciences, Beijing, China. The data matrix used in the phylogenetic analysis is provided in Supplementary Information. The CT scanning results are archived and available on Open Science Framework (https://osf.io/6jd4h/?view_only=a68708fb3f8f4a4e88494ba44f85e624) or request from the corresponding author. This published work and the nomenclatural acts it contains have been registered in ZooBank, the proposed online registration system for the International Code of Zoological Nomenclature (ICZN). The ZooBank Life Science Identifiers (LSIDs) can be resolved and the associated information viewed through any standard web browser by appending the LSID to the prefix http://zoobank.org/. The LSIDs for this publication are: urn:lsid:zoobank.org:pub:2F4C81B7-E844-470C-9D35-FFAE62F04781.

Code availability

The R code that we used in comparative analyses is archived and available on OSF (https://osf.io/6jd4h/?view_only=a68708fb3f8f4a4e88494ba44f85e624).

References

1. Brusatte, S. L., O'Connor, J. K. & Jarvis, E. D. The origin and diversification of birds. *Curr. Biol.* **25**, R888–R898 (2015).
2. Xu, X. et al. An integrative approach to understanding bird origins. *Science* **346**, 1253293 (2014).
3. Chiappe, L. M. & Meng, Q. *Birds of Stone: Chinese Avian Fossils from the Age of Dinosaurs* (Johns Hopkins Univ. Press, 2016).
4. O'Connor, J. K, Chiappe, L. M. & Bell, A. in *Living Dinosaurs: the Evolutionary History of Birds* (eds Gareth J. D. & Gary, K.) 39–114 (Wiley, 2011).
5. Field, D. J. et al. Complete *Ichthyornis* skull illuminates mosaic assembly of the avian head. *Nature* **557**, 96–100 (2018).
6. Lovette, I. J. & Fitzpatrick, J. W. *Handbook of Bird Biology*, 3rd edn (John Wiley & Sons, 2016).
7. Gauthier, J. Saurischian monophyly and the origin of birds. *Mem. Calif. Acad. Sci.* **8**, 1–55 (1986).
8. Chiappe, L. M. & Walker, C. A. in *Mesozoic Birds: Above the Heads of Dinosaurs* (eds Chiappe, L. M. & Witmer, L. M.) 448–472 (Univ. California, 2002).
9. Wang, M., Stidham, T. A. & Zhou, Z. A new clade of basal Early Cretaceous pygostylian birds and developmental plasticity of the avian shoulder girdle. *Proc. Natl Acad. Sci. USA* **115**, 10708–10713 (2018).
10. Zhou, Z., Meng, Q., Zhu, R. & Wang, M. Spatiotemporal evolution of the Jehol Biota: responses to the North China Craton destruction in the Early Cretaceous. *Proc. Natl Acad. Sci. USA* **118**, e2107859118 (2021).
11. Hone, D. W., Farke, A. A. & Wedel, M. J. Ontogeny and the fossil record: what, if anything, is an adult dinosaur? *Biol. Lett.* **12**, 20150947 (2016).
12. Plateau, O. & Foth, C. Common patterns of skull bone fusion and their potential to discriminate different ontogenetic stages in extant birds. *Frontiers Ecol. Evol.* **9**, (2021).
13. Campione, N. E., Evans, D. C., Brown, C. M. & Carrano, M. T. Body mass estimation in non-avian bipeds using a theoretical conversion to quadruped stylopodial proportions. *Methods Ecol. Evol.* **5**, 913–923 (2014).
14. Mayr, G., Pohl, B., Hartman, S. & Peters, D. S. The tenth skeletal specimen of *Archaeopteryx*. *Zool. J. Linn. Soc.* **149**, 97–116 (2007).
15. Rauhut, O. W., Foth, C. & Tischlinger, H. The oldest *Archaeopteryx* (Theropoda: Avialiae): a new specimen from the Kimmeridgian/Tithonian boundary of Schamhaupten, Bavaria. *PeerJ* **6**, e4191 (2018).
16. Xu, X. et al. The taxonomic status of the Late Cretaceous dromaeosaurid *Linheraptor exquisitus* and its implications for dromaeosaurid systematics. *Vertebr. Palasiat.* **53**, 29–62 (2015).
17. Hu, H. et al. Evolution of the vomer and its implications for cranial kinesis in Paraves. *Proc. Natl Acad. Sci. USA* **116**, 19571–19578 (2019).
18. Wang, M., Stidham, T. A., Li, Z., Xu, X. & Zhou, Z. Cretaceous bird with dinosaur skull sheds light on avian cranial evolution. *Nat. Commun.* **12**, 3890 (2021).
19. Wang, M., O'Connor, J. K. & Zhou, Z. A taxonomical revision of the Confuciusornithiformes (Aves: Pygostylia). *Vertebr. Palasiat.* **57**, 1–37 (2019).
20. O'Connor, J. K. & Chiappe, L. M. A revision of enantiornithine (Aves: Ornithothoraces) skull morphology. *J. Syst. Palaeontol.* **9**, 135–157 (2011).
21. Xu, X., Norell, M. A., Wang, X., Makovicky, P. J. & Wu, X. A basal troodontid from the Early Cretaceous of China. *Nature* **415**, 780–784 (2002).
22. Zhang, Z., Chiappe, L. M., Han, G. & Chinsamy, A. A large bird from the Early Cretaceous of China: new information on the skull of enantiornithines. *J. Vertebr. Paleontol.* **33**, 1176–1189 (2013).
23. Turner, A. H., Makovicky, P. J. & Norell, M. A. A review of dromaeosaurid systematics and paravian phylogeny. *Bull. Am. Mus. Nat. Hist.* **371**, 1–206 (2012).
24. Witmer, L. in *Encyclopedia of Dinosaurs* (eds Currie, P. J. & Padian, K.) 151–159 (Academic Press, 1997).
25. Currie, P. J. New information on the anatomy and relationships of *Dromaeosaurus albertensis* (Dinosauria: Theropoda). *J. Vertebr. Paleontol.* **15**, 576–591 (1995).
26. Xu, X., You, H., Du, K. & Han, F. An *Archaeopteryx*-like theropod from China and the origin of Avialae. *Nature* **475**, 465–470 (2011).
27. O'Connor, J. K. *A systematic review of Enantiornithes (Aves: Ornithothoraces)* (University of Southern California, 2009).
28. Norell, M. A., Clark, J. M., Turner, A. H., Makovicky, P. J., Barsbold, R. & Rowe, T. A new dromaeosaurid theropod from Ukhaa Tolgod (Ömnögov, Mongolia). *Am. Mus. Novit.* **3545**, 1–51 (2006).
29. Sullivan, C. & Xu, X. Morphological diversity and evolution of the jugal in dinosaurs. *Anat. Rec.* **300**, 30–48 (2017).
30. O'Connor, P. M. et al. Late Cretaceous bird from Madagascar reveals unique development of beaks. *Nature* **588**, 272–276 (2020).
31. Rauhut, O. W. The interrelationships and evolution of basal theropod dinosaurs. *Spec. Pap. Palaeontol.* **69**, 1–213 (2003).
32. Elzanowski, A. & Wellnhofer, P. Cranial morphology of *Archaeopteryx*: evidence from the seventh skeleton. *J. Vertebr. Paleontol.* **16**, 81–94 (1996).
33. Chiappe, L. M., Norell, M. & Clark, J. A new skull of *Gobipteryx minuta* (Aves: Enantiornithes) from the Cretaceous of the Gobi Desert. *Am. Mus. Novit.* **3346,**, 1–15 (2001).
34. Ostrom, J. H. Osteology of *Deinonychus antirrhopus*, an unusual theropod from the Lower Cretaceous of Montana. **30**, 1–165 (1969).
35. Currie, P. J. & Zhao, X. A new carnosaur (Dinosauria, Theropoda) from the Jurassic of Xinjiang, People's Republic of China. *Can. J. Earth Sci.* **30**, 2037–2081 (1993).
36. Gingerich, P. D. Evolutionary significance of the Mesozoic toothed birds. *Smithson. Contrib. Paleobiol.* **27**, 23–33 (1976).
37. McDowell, S. The bony palate of birds. Part I. The Palaeognathae. *Auk* **65**, 520–549 (1948).
38. Baumel, J. J. & Witmer, L. M. in *Handbook of Avian Anatomy: Nomina Anatomica Avium* (eds Baumel J. J. et al.) 45–132 (Nuttall Ornithological Club, 1993).
39. Zhou, Z. & Zhang, F. A long-tailed, seed-eating bird from the Early Cretaceous of China. *Nature* **418**, 405–409 (2002).

40. Vickaryous, M. K. & Hall, B. K. Homology of the reptilian coracoid and a reappraisal of the evolution and development of the amniote pectoral apparatus. *J. Anat.* **208**, 263–285 (2006).
41. Zhou, Z. & Zhang, F. *Jeholornis* compared to *Archaeopteryx*, with a new understanding of the earliest avian evolution. *Naturwissenschaften* **90**, 220–225 (2003).
42. Wang, M. & Zhou, Z. A new confuciusornithid (Aves: Pygostylia) from the Early Cretaceous increases the morphological disparity of the Confuciusornithidae. *Zool. J. Linn. Soc.* **185**, 417–430 (2019).
43. Chiappe, L. M., Ji, S. A., Ji, Q. & Norell, M. A. Anatomy and systematics of the Confuciusornithidae (Theropoda: Aves) from the Late Mesozoic of northeastern China. *Bull. Am. Mus. Nat. Hist.* **242**, 1–89 (1999).
44. O'Connor, J. K. et al. Evolution and functional significance of derived sternal ossification patterns in ornithothoracine birds. *J. Evol. Biol.* **28**, 1550–1567 (2015).
45. Chiappe, L. M. & Walker, C. A. in *Mesozoic Birds: Above the Heads of Dinosaurs* (eds Chiappe, L. M. & Witmer, L. M.) 240–267 (Univ. California, 2002).
46. Wang, M., Wang, X., Wang, Y. & Zhou, Z. A new basal bird from China with implications for morphological diversity in early birds. *Sci. Rep.* **6**, 19700 (2016).
47. Rauhut, O. W. M., Tischlinger, H. & Foth, C. A non-archaeopterygid avialan theropod from the Late Jurassic of southern Germany. *eLife* **8**, e43789 (2019).
48. Osmólska, H., Currie, P. J. & Barsbold, R. in *The Dinosauria* (eds. Weishampel, D., Dodson, P. & Osmólska, H.) 165–183 (University of California Press, 2004).
49. Hutchinson, J. R. The evolution of pelvic osteology and soft tissues on the line to extant birds (Neornithes). *Zool. J. Linn. Soc.* **131**, 123–168 (2001).
50. Wellnhofer, P. *Archaeopteryx: The Icon of Evolution* (Verlag Dr. Friedrich Pfeil, 2009).
51. Hattori, S. Evolution of the hallux in non-avian theropod dinosaurs. *J. Vertebr. Paleontol.* **36**, e1116995 (2016).
52. Zhou, Z. & Zhang, F. Anatomy of the primitive bird *Sapeornis chaoyangensis* from the Early Cretaceous of Liaoning, China. *Can. J. Earth Sci.* **40**, 731–747 (2003).
53. Botelho, J. F., Smith-Paredes, D., Soto-AcuÑA, S., NÚÑEz-LeÓN, D., Palma, V. & Vargas, A. O. Greater growth of proximal metatarsals in bird embryos and the evolution of hallux position in the grasping foot. *J. Exp. Zool.* **00**, 1–13 (2016).
54. Wang, M. et al. An Early Cretaceous enantiornithine bird with a pintail. *Curr. Biol.* **31**, 4845–4852 (2021).
55. Wang, M., Lloyd, G. T., Zhang, C. & Zhou, Z. The patterns and modes of the evolution of disparity in Mesozoic birds. *Proc. R. Soc. B* **288**, 20203105 (2021).
56. Hu, H., O'Connor, J. K. & Zhou, Z. A new species of Pengornithidae (Aves: Enantiornithes) from the Lower Cretaceous of China suggests a specialized scansorial habitat previously unknown in early birds. *PLoS ONE* **10**, e0126791 (2015).
57. O'Connor, J. K., Wang, M. & Hu, H. A new ornithuromorph (Aves) with an elongate rostrum from the Jehol Biota, and the early evolution of rostralization in birds. *J. Syst. Palaeontol.* **14**, 939–948 (2016).
58. Blomberg, S. P., Garland, T. & Ives, A. R. Testing for phylogenetic signal in comparative data: behavioral traits are more labile. *Evolution* **57**, 717–745 (2003).
59. Pagel, M. Inferring the historical patterns of biological evolution. *Nature* **401**, 877–884 (1999).
60. Holliday, C. M. & Witmer, L. M. Cranial kinesis in dinosaurs: intracranial joints, protractor muscles, and their significance for cranial evolution and function in diapsids. *J. Vertebr. Paleontol.* **28**, 1073–1088 (2008).
61. Gussekloo, S. W. S. & Bout, R. G. Cranial kinesis in palaeognathous birds. *J. Exp. Biol.* **208**, 3409–3419 (2005).
62. Plateau, O. & Foth, C. Birds have peramorphic skulls, too: anatomical network analyses reveal oppositional heterochronies in avian skull evolution. *Commun. Biol.* **3**, 195 (2020).
63. Clarke, J. A. & Norell, M. A. The morphology and phylogenetic position of *Apsaravis ukhaana* from the Late Cretaceous of Mongolia. *Am. Mus. Novit.* **3387**, 1–46 (2002).
64. Huang, R., Zhi, Q., Patel, K., Wilting, J. & Christ, B. Dual origin and segmental organisation of the avian scapula. *Development* **127**, 3789–3794 (2000).
65. Jenkins, F. A. The evolution of the avian shoulder joint. *Am. J. Sci.* **293**, 253–253 (1993).
66. Novas, F. E., Motta, M. J., Agnolín, F. L., Rozadilla, S., Lo Coco, G. E. & Brissón Egli, F. Comments on the morphology of basal paravian shoulder girdle: new data based on unenlagiid theropods and paleognath birds. *Front. Earth Sci.* **9**, (2021).
67. Ostrom, J. H. Some hypothetical anatomical stages in the evolution of avian flight. *Smithson. Contrib. Paleobiol.* **27**, 1–21 (1976).
68. Dial, K. P. Activity patterns of the wing muscles of the pigeon (*Columba livia*) during different modes of flight. *J. Exp. Zool.* **262**, 357–373 (1992).
69. Kovacs, C. E. & Meyers, R. A. Anatomy and histochemistry of flight muscles in a wing-propelled diving bird, the Atlantic Puffin, *Fratercula arctica*. *J. Morphol.* **244**, 109–125 (2000).
70. Brusatte, S. L. et al. The osteology of *Balaur bondoc*, an Island-Dwelling Dromaeosaurid (Dinosauria: Theropoda) from the Late Cretaceous of Romania. *Bull. Am. Mus. Nat. Hist.* **2013**, 1–100 (2013).
71. Romer, A. S. *Osteology of the Reptiles* (Univ. Chicago Press, 1956).
72. Gatesy, S. M. Hind limb scaling in birds and other theropods: implications for terrestrial locomotion. *J. Morphol.* **209**, 83–96 (1991).
73. Middleton, K. M. *Morphology, Evolution, and Function of the Avian Hallux* (Brown Univ., 2003).
74. Kamilar, J. M. & Cooper, N. Phylogenetic signal in primate behaviour, ecology and life history. *Philos. Trans. R. Soc. B* **368**, 20120341 (2013).
75. Goloboff, P. A. & Catalano, S. A. TNT version 1.5, including a full implementation of phylogenetic morphometrics. *Cladistics* **32**, 221–238 (2016).
76. Benson, R. B. J. et al. Rates of dinosaur body mass evolution indicate 170 million years of sustained ecological innovation on the avian stem lineage. *PLoS Biol.* **12**, e1001853 (2014).
77. Xu, X. et al. Two Early Cretaceous fossils document transitional stages in alvarezsaurian dinosaur evolution. *Curr. Biol.* **28**, 1–8 (2018).
78. Lee, Y. N. et al. Resolving the long-standing enigmas of a giant ornithomimosaur *Deinocheirus mirificus*. *Nature* **515**, 257–260 (2014).
79. Rauhut, O. W. M. & Pol, D. Probable basal allosauroid from the early Middle Jurassic Cañadón Asfalto Formation of Argentina highlights phylogenetic uncertainty in tetanuran theropod dinosaurs. *Sci. Rep.* **9**, 18826 (2019).
80. Novas, F. E., Agnolin, F. L., Ezcurra, M. D., Temp Müller, R., Martinelli, A. G. & Langer, M. C. Review of the fossil record of early dinosaurs from South America, and its phylogenetic implications. *J. S. Am. Earth Sci.* **110**, 103341 (2021).
81. Paradis, E., Claude, J. & Strimmer, K. APE: analyses of phylogenetics and evolution in R language. *Bioinformatics* **20**, 289–290 (2004).
82. Brusatte, S. L. in *Computational Paleontology* (ed. Elewa, A. M. T) 53–74 (Springer, 2011).

83. Bapst, D. W. Paleotree: an R package for paleontological and phylogenetic analyses of evolution. *Methods Ecol. Evol.* **3**, 803–807 (2012).
84. Felsenstein, J. Phylogenies and the comparative method. *Am. Nat.* **125**, 1–15 (1985).
85. Revell, L. J. Phytools: an R package for phylogenetic comparative biology (and other things). *Methods Ecol. Evol.* **3**, 217–223 (2012).
86. Blomberg, S. P., Garland, T. & Ives, A. R. Testing for phylogenetic signal in comparative data: Behavioral traits are more labile. *Evolution* **57**, 717–745 (2003).
87. Warton, D. I., Duursma, R. A., Falster, D. S. & Taskinen, S. SMATR 3—an R package for estimation and inference about allometric lines. *Methods Ecol. Evol.* **3**, 257–259 (2012).
88. Legendre, P. lmodel2. R package version 1.7-2 http://cran.r-project.org/web/packages/lmodel2/lmodel2.pdf. (2013)
89. Pinheiro, J. et al. nlme: Linear and Nonlinear Mixed EffectsModels. *R package version 3.1-158* https://svn.r-project.org/R-packages/trunk/nlme/ (2022)
90. Dececchi, T. A. & Larsson, H. C. E. Assessing arboreal adaptations of bird antecedents: testing the ecological setting of the origin of the avian flight stroke. *PLoS ONE* **6**, e22292 (2011).
91. Hastie, T., Tibshirani, R., Leisch, F., Hornik, K. & Ripley, B. mda: mixture and flexible discriminant analysis. *R package version 0.5-3* https://cran.r-project.org/package=mda (2022).

Acknowledgements

We thank P. Yin for help with CT scanning, and W. Gao for photographing. This research is supported by the National Natural Science Foundation of China (42288201), the Key Research Program of Frontier Sciences, CAS (ZDBS-LY-DQC002) and the Tencent Foundation (through the XPLORER PRIZE).

Author contributions

M.W. conceived the project; Z.L. and M.W. conducted the digital reconstruction; M.W. collected the data; M.W. performed the phylogenetic analysis and comparative analyses; M.W., Z.L., T.A.S. and Z.Z. wrote the manuscript.

Competing interests

The authors declare no competing interests.

Additional information

Extended data is available for this paper at https://doi.org/10.1038/s41559-022-01921-w.

Supplementary information The online version contains supplementary material available at https://doi.org/10.1038/s41559-022-01921-w.

Correspondence and requests for materials should be addressed to Min Wang.

Peer review information *Nature Ecology & Evolution* thanks Fernando Novas and the other, anonymous, reviewer(s) for their contribution to the peer review of this work.

https://doi.org/10.1038/s41559-022-01921-w

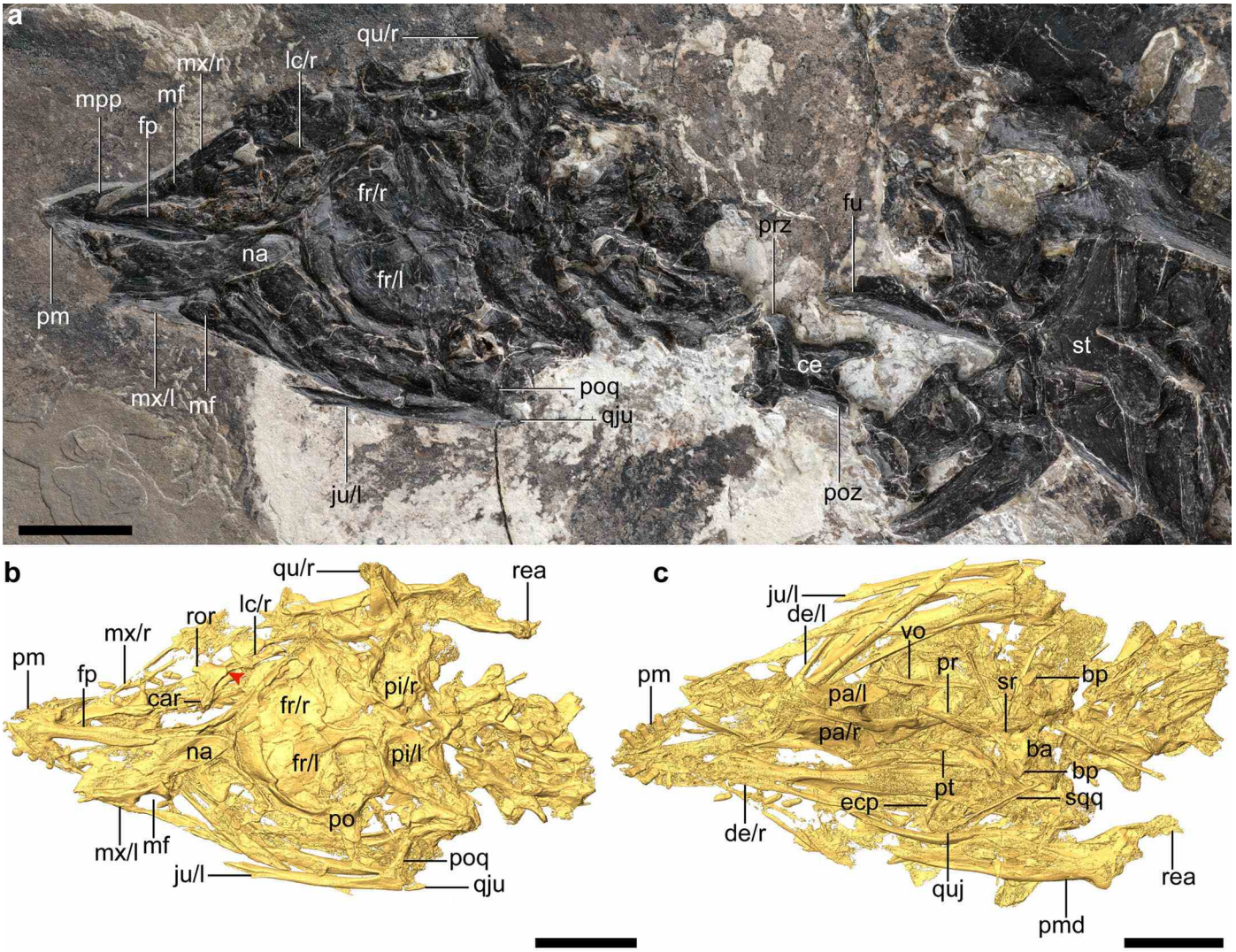

Extended Data Fig. 1 | Additional cranial anatomy of *Cratonavis zhui*, IVPP V31106. **a**, Photograph. **b, c**, CT Isosurface of the whole skull in dorsal (**a**) and (**b**) ventral views. ba, basisphenoid-parasphenoid; bp, basipterygoid process; car, caudal ramus of lacrimal; de, dentary; ecp, ectopterygoid; fp, frontal process of premaxilla; fr, frontal; jmx, jugal process of maxilla; ju, jugal; jup, jugal process of postorbital; lc, lacrimal; mx, maxilla; na, nasal; pa, palatine; pi, parietal; pm, premaxilla; pmd, post-dentary mandible; po, postorbital; poq, postorbital process of jugal; pr, parasphenoid rostrum; pt, pterygoid; qju, quadratojugal process of jugal; qu, quadrate; quj, quadratojugal; rea, retroarticular process; sqq, squamosal process of quadratojugal; sr, subcellar recess; vo, vomer; l/r, left/right side. The arrowhead (**a**) denotes the lateral flange of the lacrimal. Scale bars, 10 mm (**a**–**c**).

https://doi.org/10.1038/s41559-022-01921-w

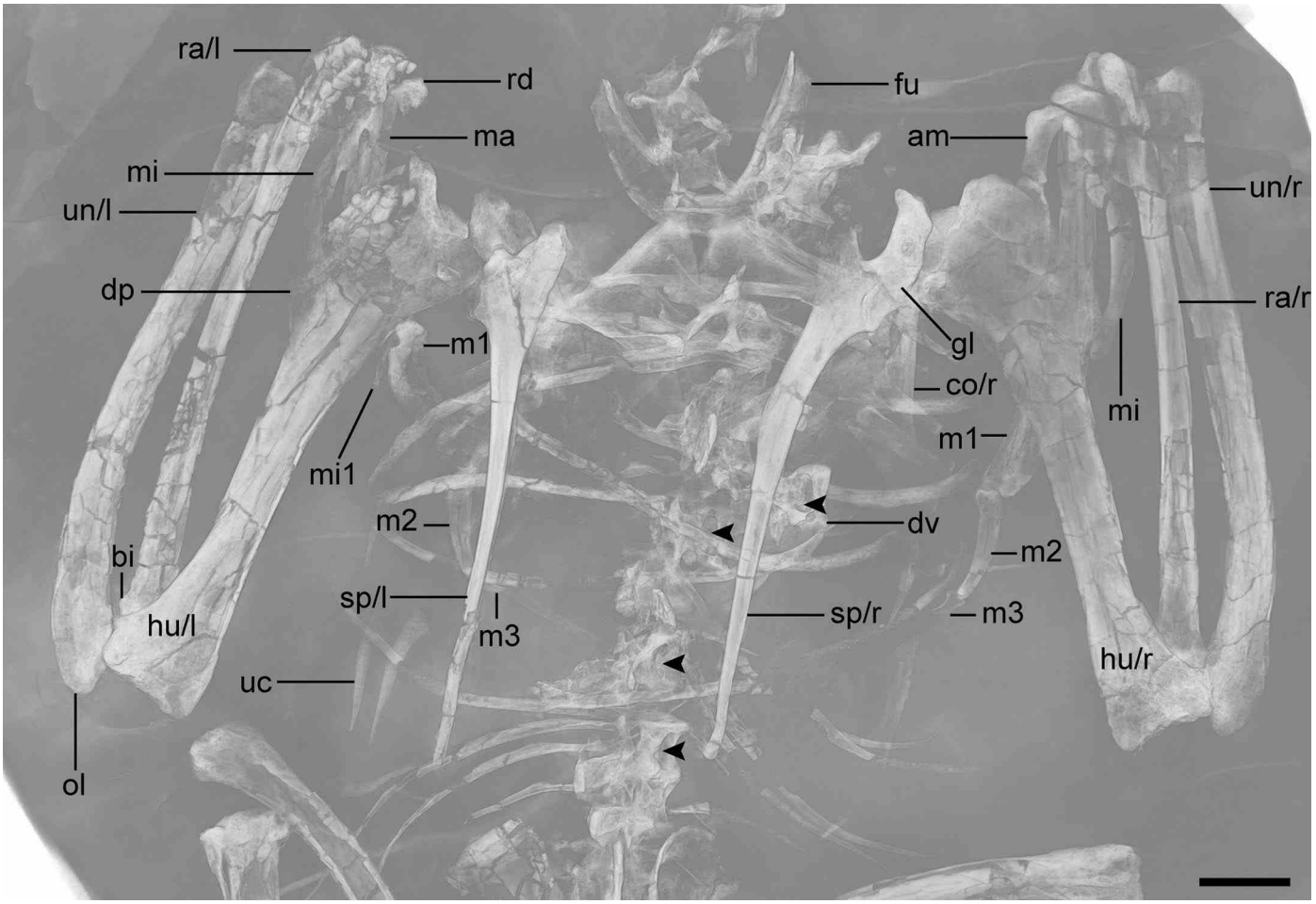

Extended Data Fig. 2 | CT scanning of pectoral region of *C. zhui*. am, alular metacarpal; bi, bicipital tubercle; co, coracoid; dp, deltopectoral crest; dv, dorsal vertebra; fu, furcula; gl, glenoid; hu, humerus; ma, major metacarpal; m1 to m3, major digit phalanx 1 to 3; mi, minor metacarpal; mi1, minor digit phalanx 1; ol, olecranon; ra, radius; rd, radiale; sp, scapula; uc, uncinate; un, ulna; l/r, left/right side. The arrowheads denote the lateral fossae of the dorsal centra. Scale bar, 10 mm.

https://doi.org/10.1038/s41559-022-01921-w

Extended Data Fig. 3 | Additional pelvis and hindlimb anatomy of *C. zhui*. **a**, Photograph. **b**, CT Scanning. fe, femur; fi, fibula; il, ilium; isp, ischiatic peduncle; mt I–V, metatarsal I to V; pop, postacetabular process; prp, preacetabular process; pt, posterior trochanter; pu, pubis; pup, pubic peduncle; py, pygostyle; ti, tibiotarsus; 1–8, sacral vertebrae one to eight; l/r, left/right side. Scale bar, 10 mm.

https://doi.org/10.1038/s41559-022-01921-w

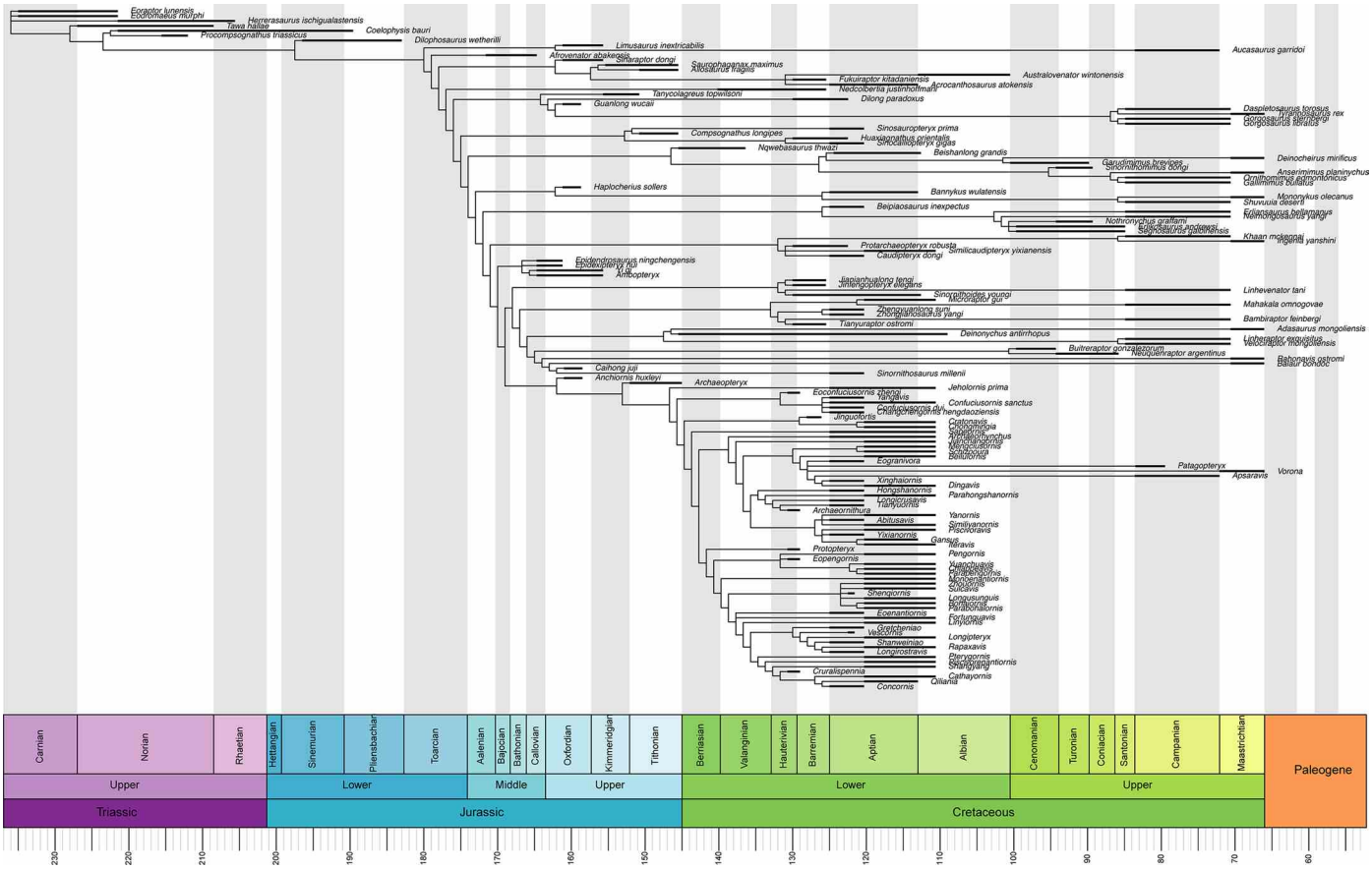

Extended Data Fig. 4 | Time-calibrated phylogeny of theropod dinosaurs. The phylogeny is a super tree encompassing major theropod groups that preserve complete appendicular elements used as the backbone for comparative analysis (see Methods).

https://doi.org/10.1038/s41559-022-01921-w

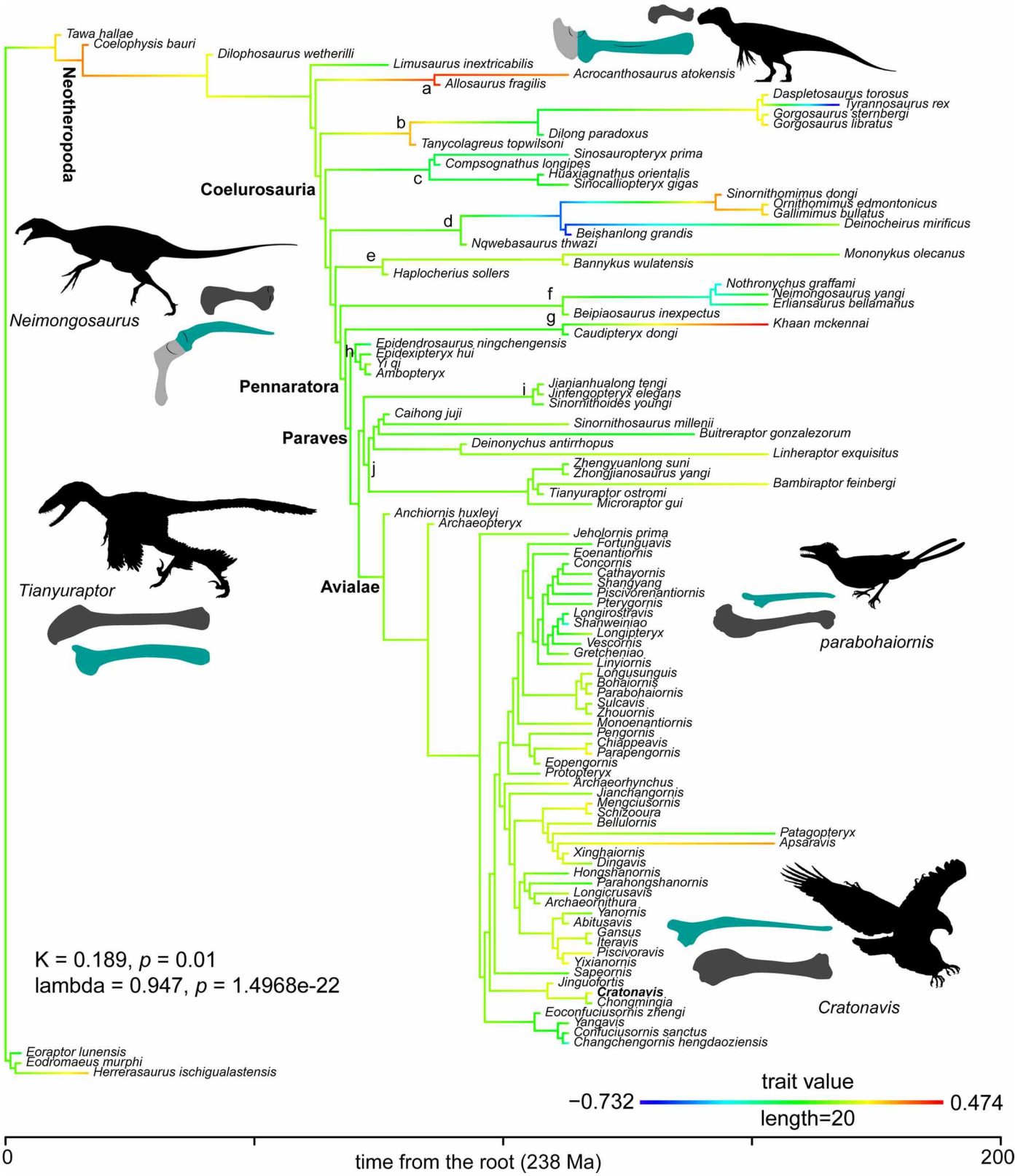

Extended Data Fig. 5 | Evolution of scapula across theropod dinosaurs. Scapula length changes among major theropod groups (line drawing of scapulocoracoid/scapula scaled with humerus in selected taxa). The phylogenetical signals were quantified using the Blomberg's *K* and Pagel's lambd with *P*-value of the likelihood radio test. Node name: a: Allosauroidea, b: Tyrannosauroidae, c: Compsognathidae, d: Therizinosauria, e: Alvarezsauria, f: Ornithomimosauria, g: Oviraptorosauria, h: Scansoriopterygidae, i: Troodontidae, j: Dromaeosauridae.

https://doi.org/10.1038/s41559-022-01921-w

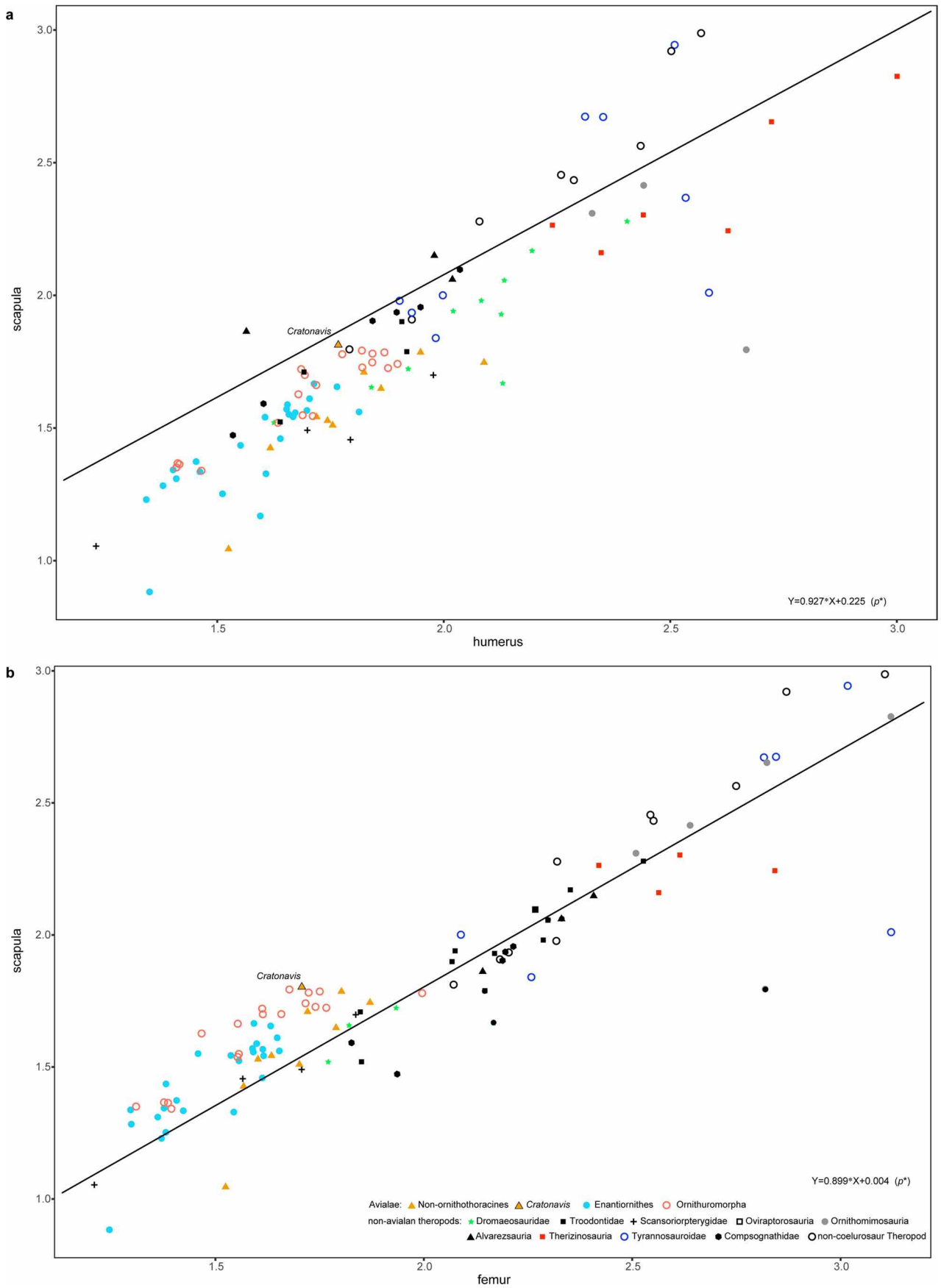

Extended Data Fig. 6 | Scaling relationship between scapula and humerus/femur length across theropod dinosaurs using phylogenetic generalized least squares (pgls). a, Scapula against humerus. **b**, Scapula against femur. Statistically significant relationship is denoted by *p*-value (*<0.01).

https://doi.org/10.1038/s41559-022-01921-w

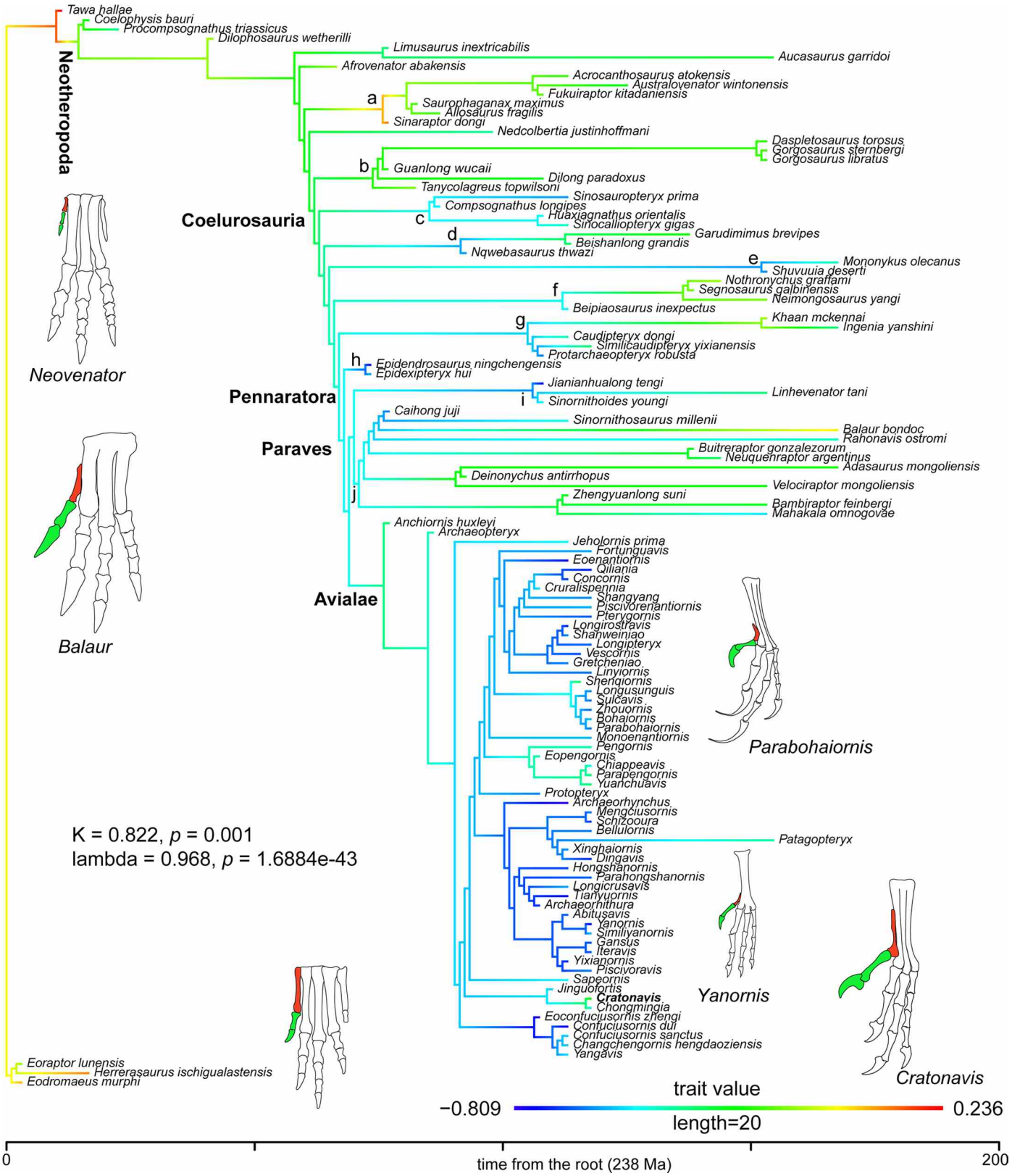

Extended Data Fig. 7 | Evolution of metatarsals across theropod dinosaurs. Changes of metatarsal I length along the line to early avialans (metatarsal I and hallux colored in red and green, respectively). The phylogenetical signals were quantified using the Blomberg's *K* and Pagel's lambd with *P*-value of the likelihood radio test. Node name: a: Allosauroidea, b: Tyrannosauroidae, c: Compsognathidae, d: Therizinosauria, e: Alvarezsauria, f: Ornithomimosauria, g: Oviraptorosauria, h: Scansoriorpterygidae, i: Troodontidae, j: Dromaeosauridae.

https://doi.org/10.1038/s41559-022-01921-w

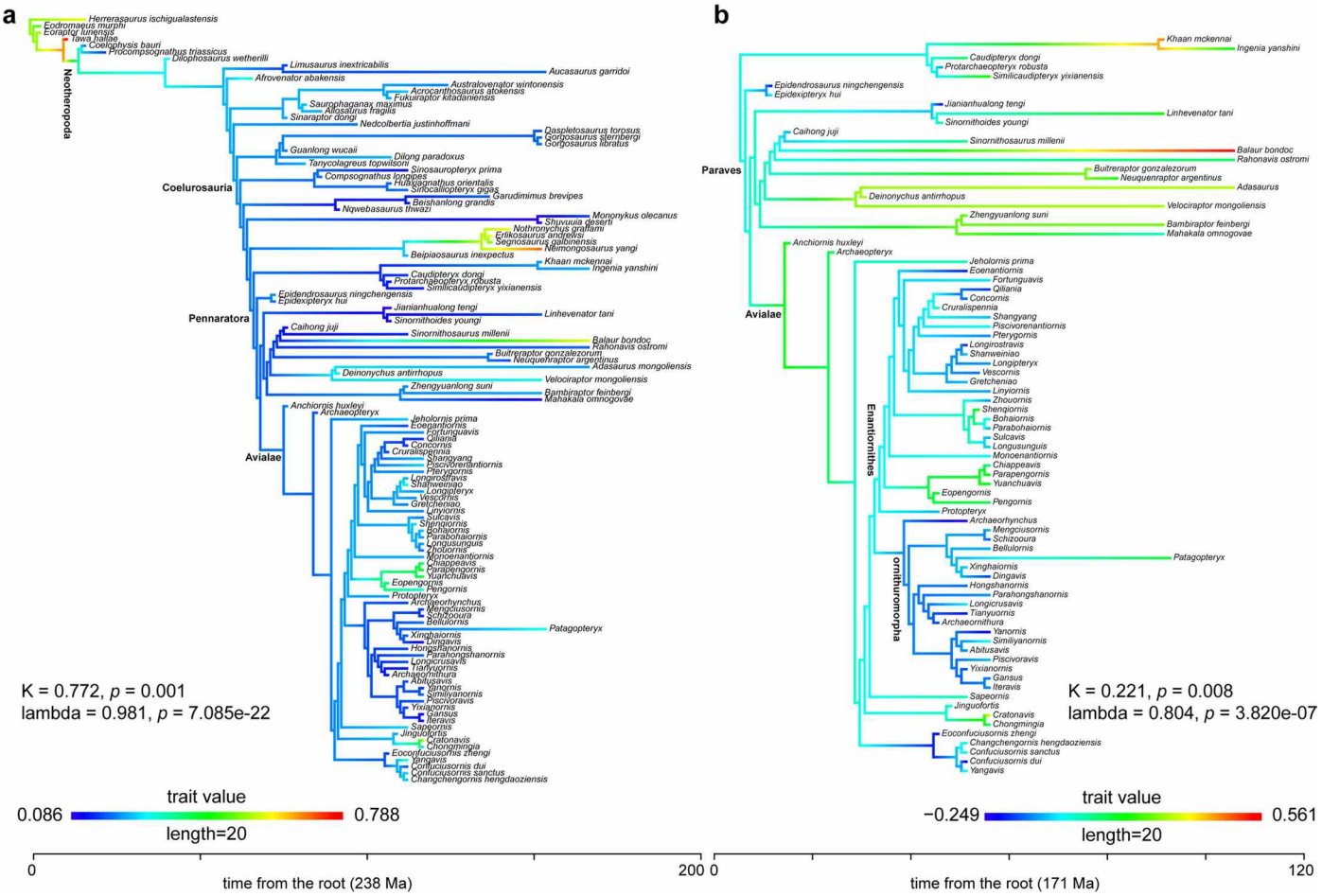

Extended Data Fig. 8 | Changes of metatarsal I length across theropod dinosaurs. a, Metatarsals I/III length ratio mapped onto time-calibrated theropod phylogeny. **b**, Size and phylogenetically corrected metatarsal I length mapped onto time-calibrated paravian phylogeny. The phylogenetical signals were quantified using the Blomberg's *K* and Pagel's lambd with *P*-value of the likelihood radio test.

https://doi.org/10.1038/s41559-022-01921-w

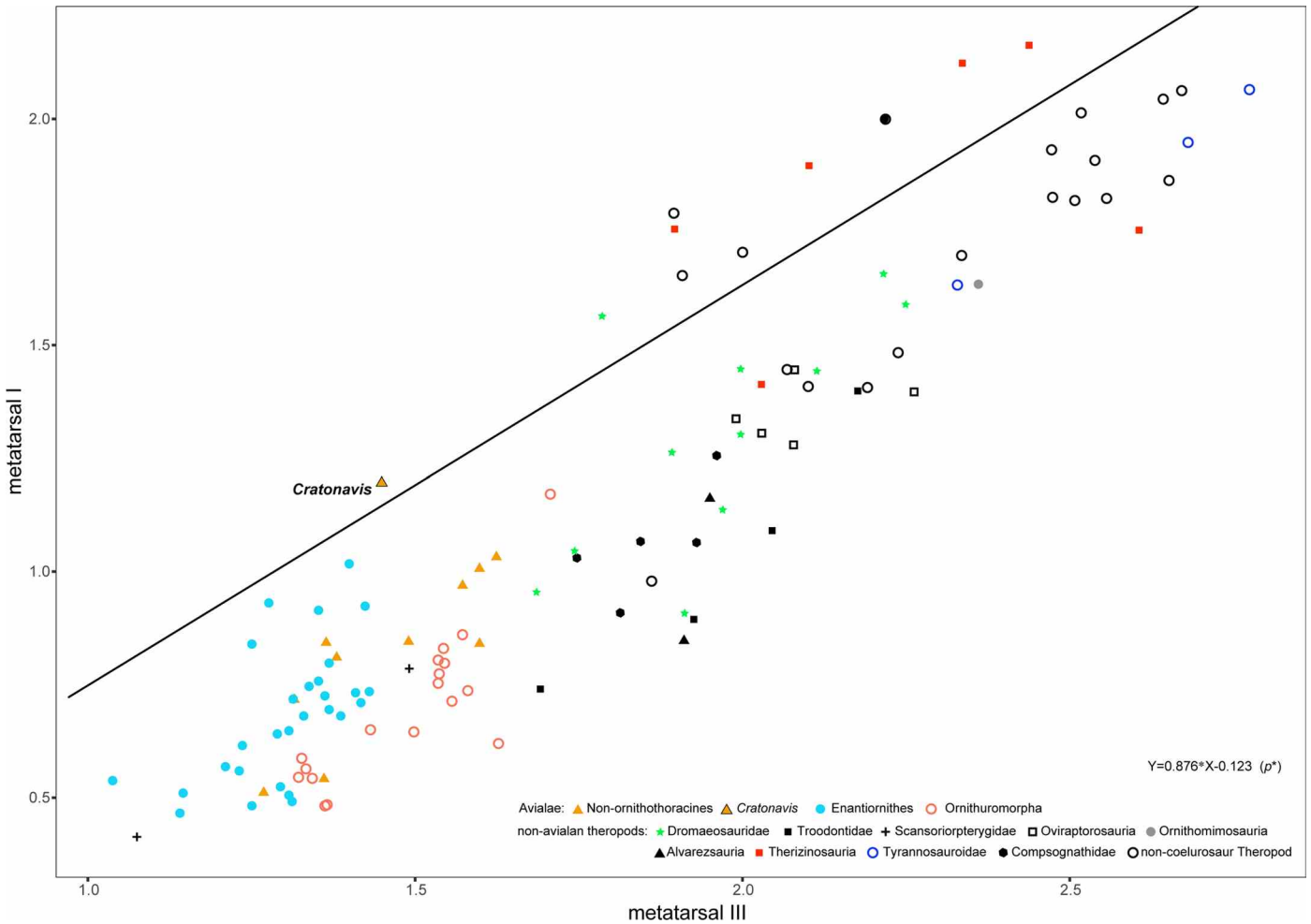

Extended Data Fig. 9 | Scaling relationship between metatarsals I and III length across theropod dinosaurs. Results using the phylogenetic generalized least squares regression (pgls). Statistically significant relationship is denoted by *p*-value (*<0.01).

https://doi.org/10.1038/s41559-022-01921-w

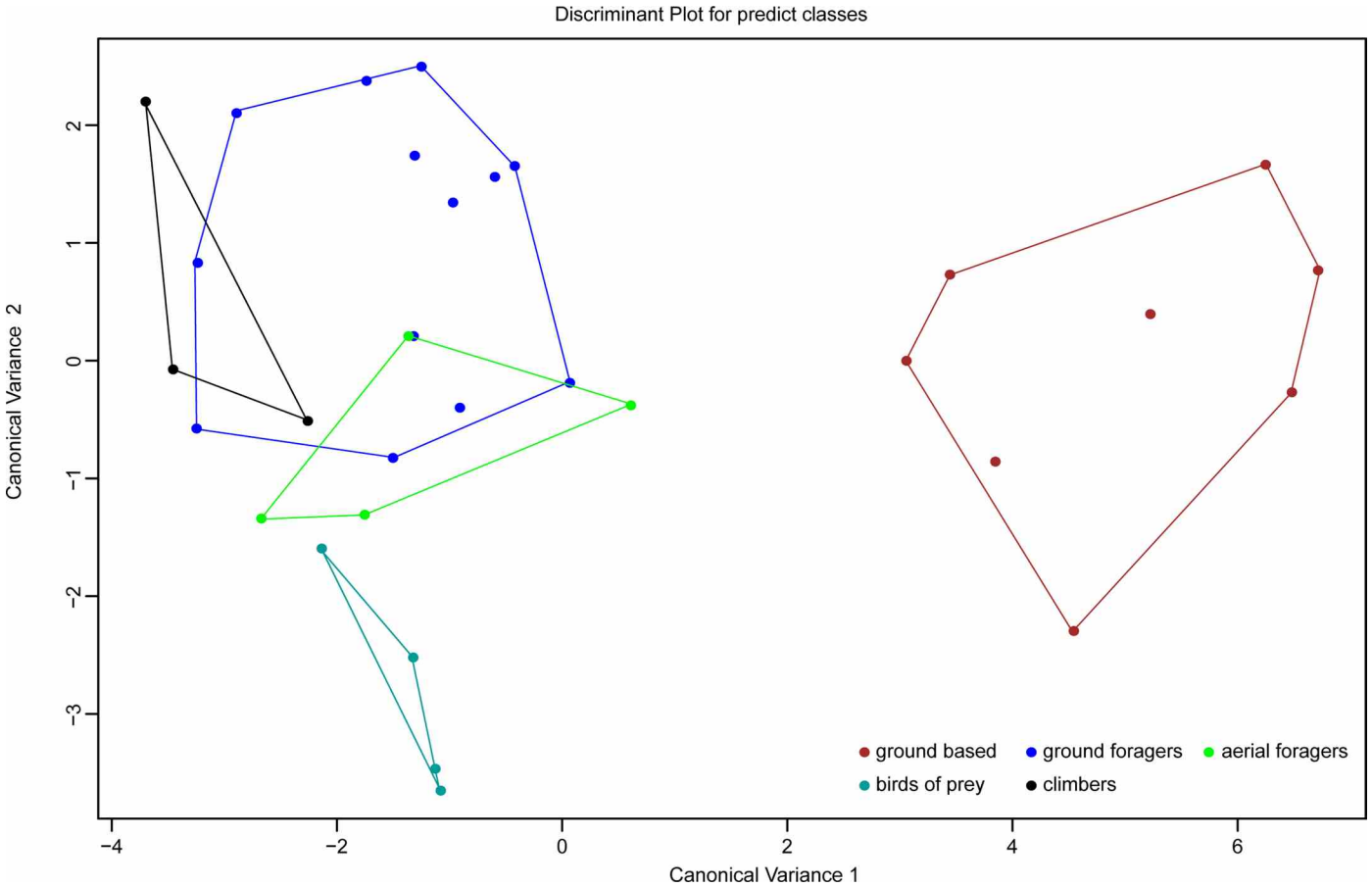

Extended Data Fig. 10 | Results of canonical variate analysis to predicate the ecologies of modern bird samples. The modern samples can be 87.5% correctly assigned to their original ecological classifications using selected morphological traits.

nature portfolio

Corresponding author(s): MIN WANG

Last updated by author(s): Sep 23, 2022

Reporting Summary

Nature Portfolio wishes to improve the reproducibility of the work that we publish. This form provides structure for consistency and transparency in reporting. For further information on Nature Portfolio policies, see our Editorial Policies and the Editorial Policy Checklist.

Statistics

For all statistical analyses, confirm that the following items are present in the figure legend, table legend, main text, or Methods section.

n/a	Confirmed	
☒	☐	The exact sample size (*n*) for each experimental group/condition, given as a discrete number and unit of measurement
☒	☐	A statement on whether measurements were taken from distinct samples or whether the same sample was measured repeatedly
☒	☐	The statistical test(s) used AND whether they are one- or two-sided *Only common tests should be described solely by name; describe more complex techniques in the Methods section.*
☒	☐	A description of all covariates tested
☒	☐	A description of any assumptions or corrections, such as tests of normality and adjustment for multiple comparisons
☒	☐	A full description of the statistical parameters including central tendency (e.g. means) or other basic estimates (e.g. regression coefficient) AND variation (e.g. standard deviation) or associated estimates of uncertainty (e.g. confidence intervals)
☒	☐	For null hypothesis testing, the test statistic (e.g. *F*, *t*, *r*) with confidence intervals, effect sizes, degrees of freedom and *P* value noted *Give P values as exact values whenever suitable.*
☒	☐	For Bayesian analysis, information on the choice of priors and Markov chain Monte Carlo settings
☒	☐	For hierarchical and complex designs, identification of the appropriate level for tests and full reporting of outcomes
☒	☐	Estimates of effect sizes (e.g. Cohen's *d*, Pearson's *r*), indicating how they were calculated

Our web collection on statistics for biologists contains articles on many of the points above.

Software and code

Policy information about availability of computer code

Data collection	Photographs of the fossils were taken using a Nikon D850 Camera. Specimens were industrial scanned using the industrial CT scanner Phoenix v-tome-x at the Institute of Vertebrate Paleontology.
Data analysis	The ct scanned data were imported into Avizo (version 9.2.0) for digital segmentation, rendering, and reconstruction; phylogenetic analysis were conducted using the TNT v. 1.5 software package. R v 4.0.3 software was used in the phylogenetic comparative analyses.

For manuscripts utilizing custom algorithms or software that are central to the research but not yet described in published literature, software must be made available to editors and reviewers. We strongly encourage code deposition in a community repository (e.g. GitHub). See the Nature Portfolio guidelines for submitting code & software for further information.

Data

Policy information about availability of data

All manuscripts must include a data availability statement. This statement should provide the following information, where applicable:

- Accession codes, unique identifiers, or web links for publicly available datasets
- A description of any restrictions on data availability
- For clinical datasets or third party data, please ensure that the statement adheres to our policy

The specimen (IVPP V31106) described in this study is archived and available on request from the Institute of Vertebrate Paleontology and Paleoanthropology (IVPP), Chinese Academy of Sciences, Beijing, China. The CT scanning results are archived and available on Open Science Framework (OSF), or request from the

corresponding author. Data matrix used in the phylogenetic analysis is provided in the Supplementary Information. The R code that we used in comparative analyses is available at OSF.

Human research participants

Policy information about studies involving human research participants and Sex and Gender in Research.

Reporting on sex and gender	not applicable
Population characteristics	not applicable
Recruitment	not applicable
Ethics oversight	not applicable

Note that full information on the approval of the study protocol must also be provided in the manuscript.

Field-specific reporting

Please select the one below that is the best fit for your research. If you are not sure, read the appropriate sections before making your selection.

☐ Life sciences ☐ Behavioural & social sciences ☒ Ecological, evolutionary & environmental sciences

For a reference copy of the document with all sections, see nature.com/documents/nr-reporting-summary-flat.pdf

Ecological, evolutionary & environmental sciences study design

All studies must disclose on these points even when the disclosure is negative.

Study description	Comparative anatomy of an Early Cretaceous bird fossil
Research sample	One fossil specimen.
Sampling strategy	No sample size calculation was performed.
Data collection	The specimen was discovered in the Early Cretaceous Jiufotang Formation (120 Ma) near Xiaotaizi Village, Lamadong Town, Jianchang Country, Liaoning Province, northeastern China
Timing and spatial scale	not applicable
Data exclusions	not applicable
Reproducibility	The specimen (IVPP V31106) described in this study is archived and available on request from the Institute of Vertebrate Paleontology and Paleoanthropology (IVPP), Chinese Academy of Sciences, Beijing, China. The CT scanning results are archived and available on Open Science Framework (OSF), or request from the corresponding author. Data matrix used in the phylogenetic analysis is provided in the Supplementary Information. The R code that we used in comparative analyses is available at OSF
Randomization	not applicable
Blinding	not applicable

Did the study involve field work? ☐ Yes ☒ No

Reporting for specific materials, systems and methods

We require information from authors about some types of materials, experimental systems and methods used in many studies. Here, indicate whether each material, system or method listed is relevant to your study. If you are not sure if a list item applies to your research, read the appropriate section before selecting a response.

Materials & experimental systems

n/a	Involved in the study
☒	☐ Antibodies
☒	☐ Eukaryotic cell lines
☐	☒ Palaeontology and archaeology
☒	☐ Animals and other organisms
☒	☐ Clinical data
☒	☐ Dual use research of concern

Methods

n/a	Involved in the study
☒	☐ ChIP-seq
☒	☐ Flow cytometry
☒	☐ MRI-based neuroimaging

Palaeontology and Archaeology

Specimen provenance	The specimen was discovered by the field team of the Institute of Vertebrate Paleontology and Paleoanthropology from the Early Cretaceous Jiufotang Formation (120 Ma) near Xiaotaizi Village, Lamadong Town, Jianchang Country, Liaoning Province, northeastern China
Specimen deposition	The specimen (IVPP V31106) described in this study is archived and available on request from the Institute of Vertebrate Paleontology and Paleoanthropology (IVPP), Chinese Academy of Sciences, Beijing, China.
Dating methods	No new dates were obtained for this study

☒ Tick this box to confirm that the raw and calibrated dates are available in the paper or in Supplementary Information.

Ethics oversight	The fossil specimen was collected by the field team of the Institute of Vertebrate Paleontology and Paleoanthropology, which is in compliance with permits issued by the local government and Chinese Academy of Sciences. All authors declare no competing interests.

Note that full information on the approval of the study protocol must also be provided in the manuscript.